The Galactic Center as a laboratory for alternative theories of gravity and new physics

А.Ф. Захаров (Alexander F. Zakharov)

- **E-mail: zakharov@itep.ru**
-
- ***Institute of Theoretical and Experimental Physics,***
- ***B. Cheremushkinskaya, 25, 117218 Moscow***

- ***Bogoliubov Laboratory of Theoretical Physics***
- ***Joint Institute for Nuclear Research, Dubna, Russia***

- Sixteenth Lomonosov Conference on Elementary Particle Physics
- 26 August, 2013

Mikhail Polikarpov (ITEP) 28.12.1951 – 18.07.2013

Outline of my talk

- Introduction
- Shadows for Kerr as a tool to evaluate BH characteristics
- Shadows around Reissner-Nordstrom BHs
- Observations of BH at Sgr A and a tidal Reissner-Nordstrom BH
- Bright star trajectories around BH at GC as a tool to evaluate BH parameters and DM cluster
- Conclusions

References

- AFZ, F. De Paolis, G. Ingrosso, and A. A. Nucita, New Astronomy Reviews, **56**, 64 (2012).

- D. Borka, P. Jovanovic, V. Borka Jovanovic and AFZ, Physical Reviews D, **85**, 124004 (2012).

ARTICLE IN PRESS

New Astronomy Reviews xxx (2011) xxx–xxx

Contents lists available at SciVerse ScienceDirect

New Astronomy Reviews

journal homepage: www.elsevier.com/locate/newastrev

Shadows as a tool to evaluate black hole parameters and a dimension of spacetime

Alexander F. Zakharov [a,b,*], Francesco De Paolis [c], Gabriele Ingrosso [c], Achille A. Nucita [c]

[a] Institute of Theoretical and Experimental Physics, 25, B. Cheremushkinskaya St., Moscow 117259, Russia
[b] Bogoliubov Laboratory of Theoretical Physics, Joint Institute for Nuclear Research, Dubna, Russia
[c] Dipartimento di Fisica Universita di Salento and INFN, Sezione di Lecce, Italy

ARTICLE INFO

Article history:
Available online xxxx

ABSTRACT

Shadow formation around supermassive black holes were simulated. Due to enormous progress in observational facilities and techniques of data analysis researchers approach to opportunity to measure shapes and sizes of the shadows at least for the closest supermassive black hole at the Galactic Center. Measurements of the shadow sizes around the black holes can help to evaluate parameters of black hole metric. Theories with extra dimensions (Randall–Sundrum II braneworld approach, for instance) admit astrophysical objects (supermassive black holes, in particular) which are rather different from standard ones. Different tests were proposed to discover signatures of extra dimensions in supermassive black holes since the gravitational field may be different from the standard one in the general relativity (GR) approach. In particular, gravitational lensing features are different for alternative gravity theories with extra dimensions and general relativity. Therefore, there is an opportunity to find signatures of extra dimensions in supermassive black holes. We show how measurements of the shadow sizes can put constraints on parameters of black hole in spacetime with extra dimensions.

Contents

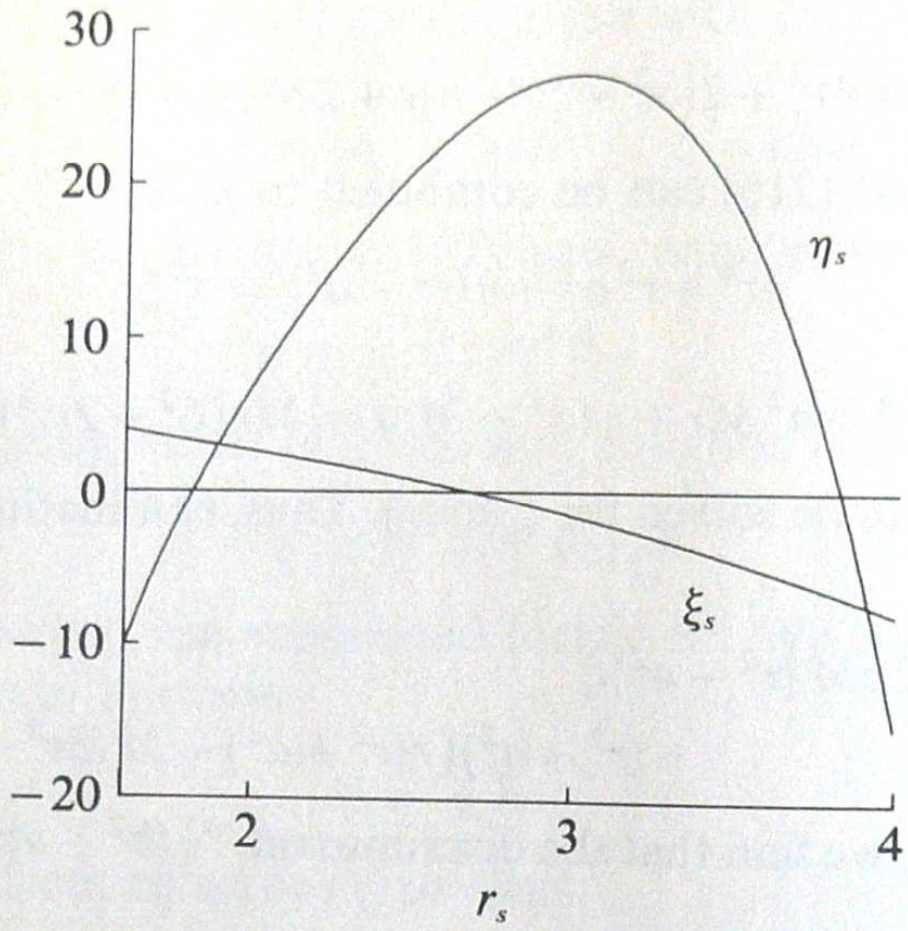

FIG. 34. The locus (ξ_s, η_s) determining the constants of the motion for three-dimensional orbits of constant radius described around a Kerr black-hole with $a = 0.8$. The unit of length along the abscissa is M.

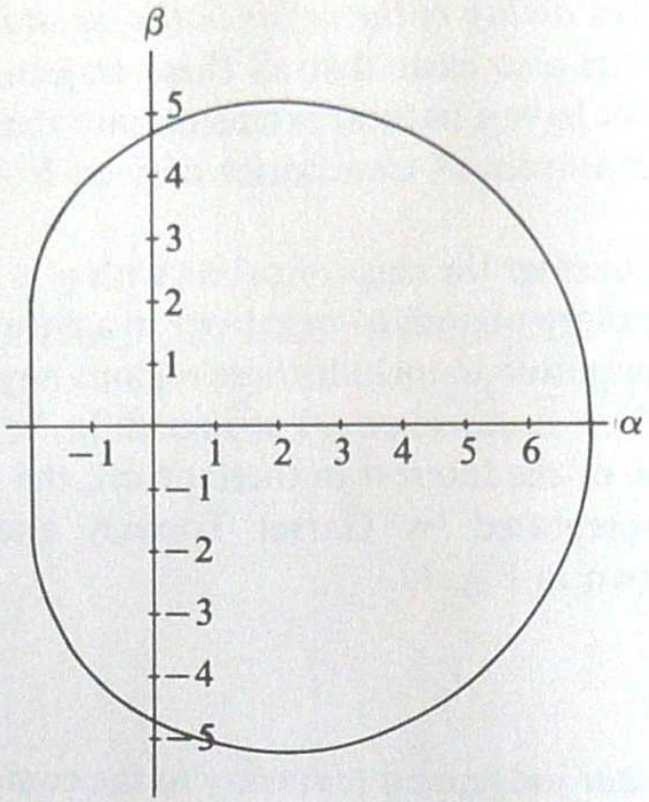

FIG. 38. The apparent shape of an extreme ($a = M$) Kerr black-hole as seen by a distant observer in the equatorial plane, if the black hole is in front of a source of illumination with an angular size larger than that of the black hole. The unit of length along the coordinate axes α and β (defined in equation (241) is M.

black hole from infinity, the apparent shape will be determined by

$$(\alpha, \beta) = [\xi, \sqrt{\eta(\xi)}]. \tag{242}$$

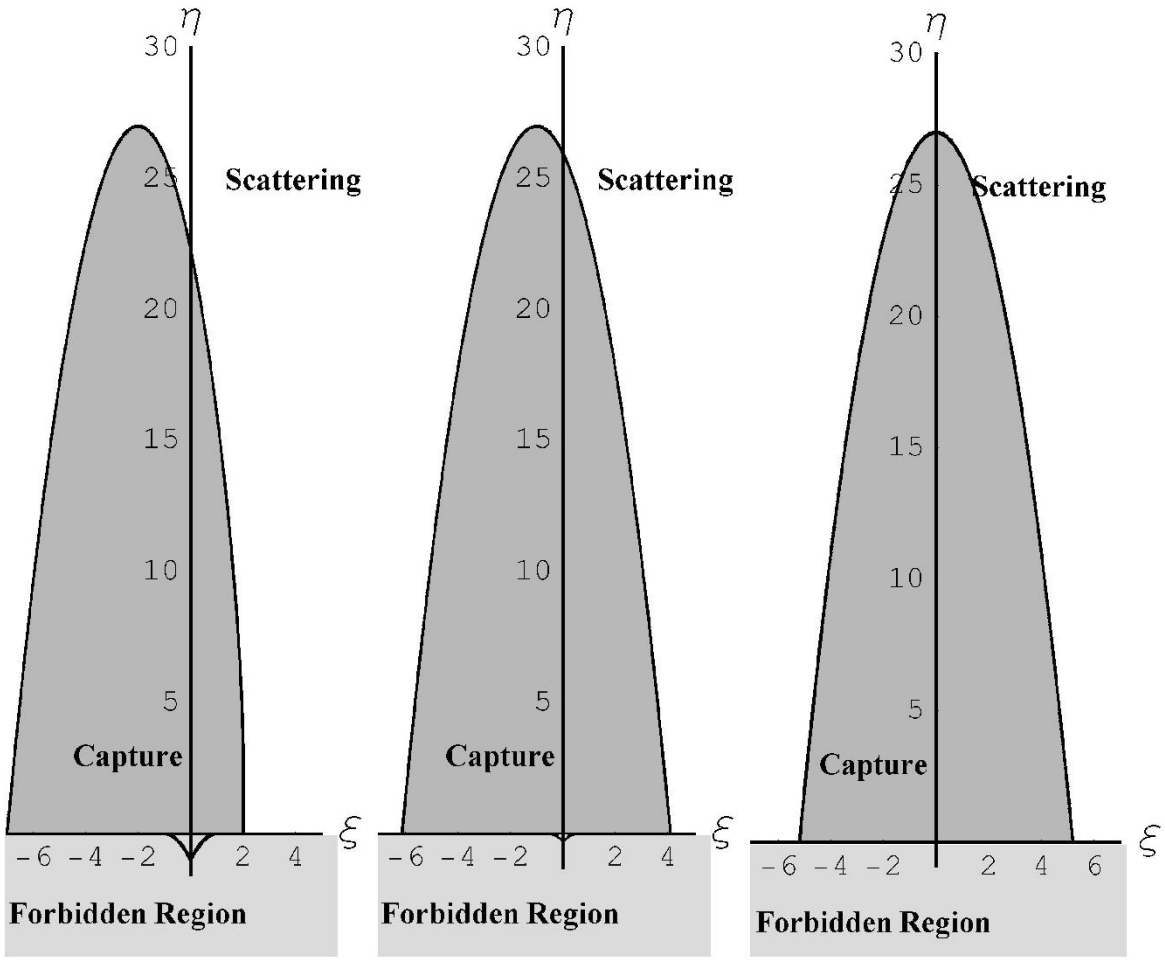

Fig. 1. Different types for photon trajectories and spin parameters ($a = 1., a = 0.5, a = 0.$). Critical curves separate capture and scatter regions. Here we show also the forbidden region corresponding to constants of motion $\eta < 0$ and $(\xi, \eta) \bar{\in} M$ as it was discussed in the text.

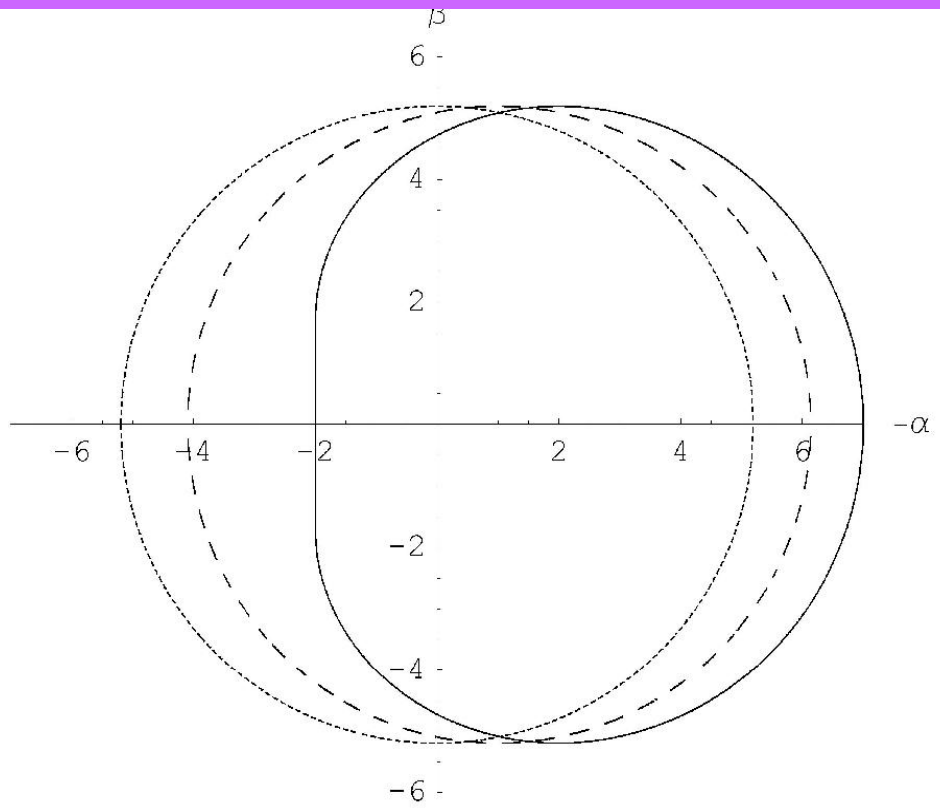

Fig. 2. Mirages around black hole for equatorial position of distant observer and different spin parameters. The solid line, the dashed line and the dotted line correspond to $a = 1, a = 0.5, a = 0$ correspondingly

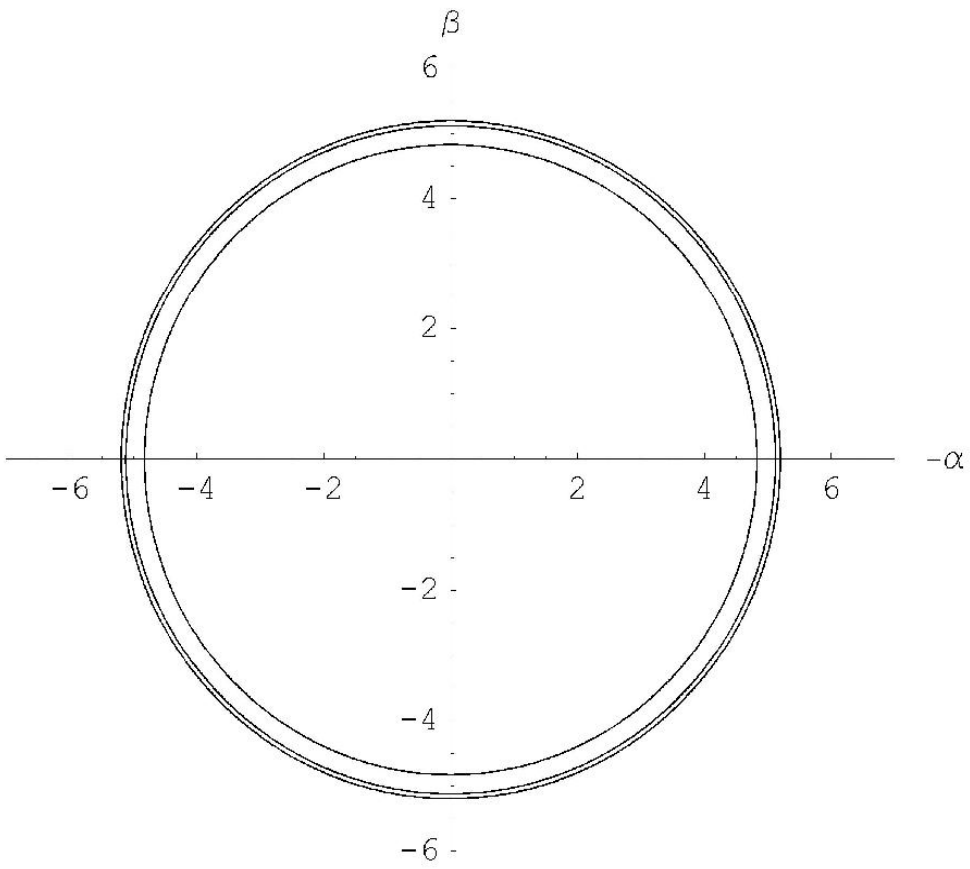

Fig. 3. Mirages around a black hole for the polar axis position of distant observer and different spin parameters ($a = 0, a = 0.5, a = 1$). Smaller radii correspond to greater spin parameters.

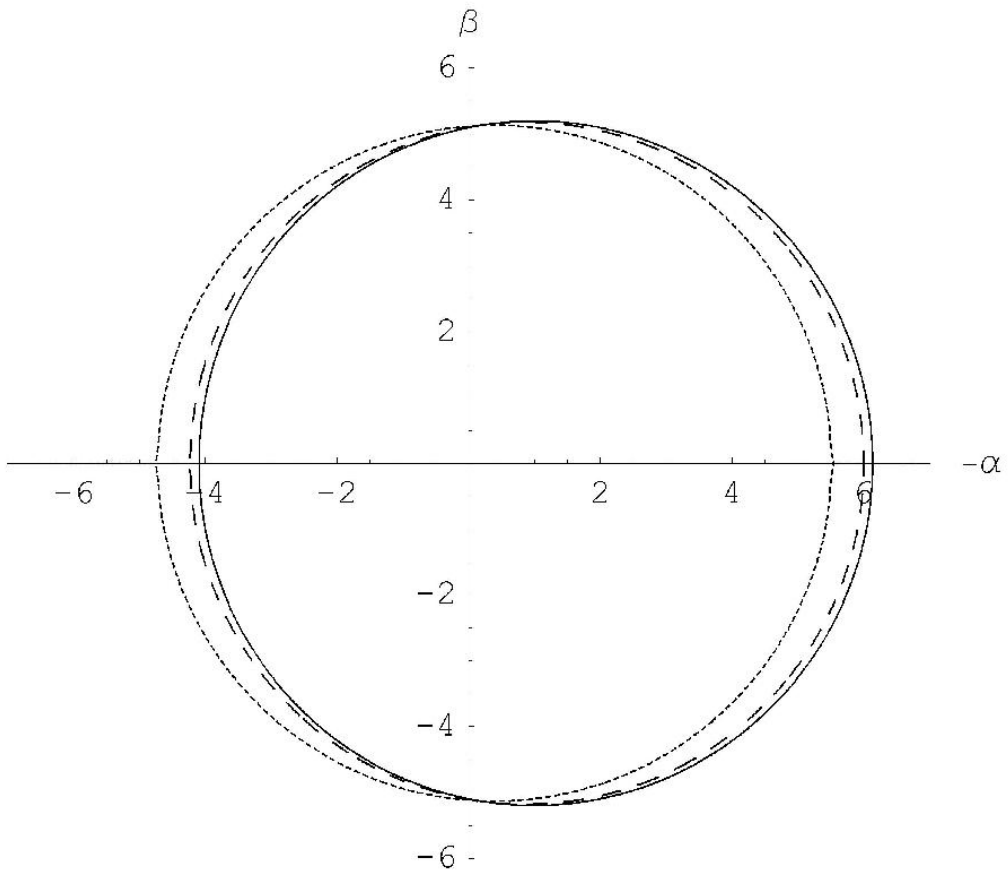

Fig. 4. Mirages around black hole for different angular positions of a distant observer and the spin $a = 0.5$. Solid, dashed and dotted lines correspond to $\theta_0 = \pi/2, \pi/3$ and $\pi/8$, respectively.

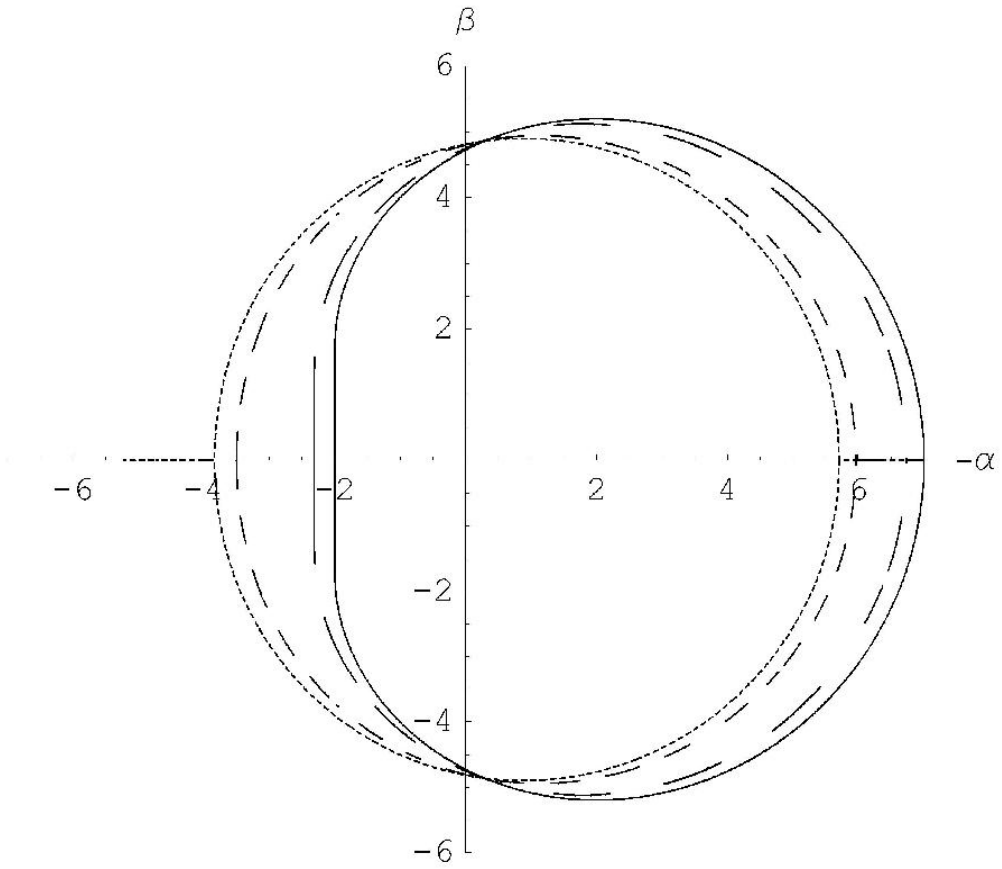

Fig. 5. Mirages around black hole for different angular positions of a distant observer and the spin $a = 1$. Solid, long dashed, short dashed and dotted lines correspond to $\theta_0 = \pi/2, \pi/3, \pi/6$ and $\pi/8$, respectively.

Direct Measurements of Black Hole Charge with Future Astrometrical Missions

A.F. Zakharov[1,2,3], F. De Paolis[4], G. Ingrosso[4], A.A. Nucita[4]

[1] Institute of Theoretical and Experimental Physics, 25, B.Cheremushkinskaya st., Moscow, 117259, Russia,

[2] Astro Space Centre of Lebedev Physics Institute, 84/32, Profsoyuznaya st., Moscow, 117810, Russia,

[3] Joint Institute for Nuclear Research, Dubna, Russia

[4] Department of Physics, University of Lecce and INFN, Section of Lecce, Via Arnesano, I-73100 Lecce, Italy

Received / accepted

Abstract. Recently, Zakharov et al. (2005a) considered the possibility of evaluating the spin parameter and the inclination angle for Kerr black holes in nearby galactic centers by using future advanced astrometrical instruments. A similar approach which uses the characteristic properties of gravitational retro-lensing images can be followed to measure the charge of Reissner-Nordström black hole. Indeed, in spite of the fact that their formation might be problematic, charged black holes are objects of intensive investigations. From the theoretical point of view it is well-known that a black hole is described by only three parameters, namely, its mass M, angular momentum J and charge Q. Therefore, it would be important to have a method for measuring all these parameters, preferably by model independent way. In this paper, we propose a procedure to measure the black hole charge by using the size of the retro-lensing images that can be revealed by future astrometrical missions. A discussion of the Kerr-Newmann black hole case is also offered.

$$R(r_{max}) = 0, \qquad \frac{\partial R}{\partial r}(r_{max}) = 0, \tag{6}$$

as it was done, for example, by Chandrasekhar (1983) to solve similar problems.

Introducing the notation $\xi^2 = l, Q^2 = q$, we obtain

$$R(r) = r^4 - lr^2 + 2lr - qr. \tag{7}$$

The discriminant Δ of the polynomial $R(r)$ has the form (as it was shown by Zakharov (1991a,b, 1994a)):

$$\Delta = 16l^3[l^2(1-q) + l(-8q^2 + 36q - 27) - 16q^3]. \tag{8}$$

The polynomial $R(r)$ thus has a multiple root if and only if

$$l^3[l^2(1-q) + l(-8q^2 + 36q - 27) - 16q^3] = 0. \tag{9}$$

Excluding the case $l = 0$, which corresponds to a multiple root at $r = 0$, we find that the polynomial $R(r)$ has a multiple root for $r \geq r_+$ if and only if

$$l^2(1-q) + l(-8q^2 + 36q - 27) - 16q^3 = 0. \tag{10}$$

If $q = 0$, we obtain the well-known result for a Schwarzschild black hole (Misner, Thorne and Wheeler 1973; Wald 1984; Lightman et al. 1975), $l = 27$, or $L_{cr} = 3\sqrt{3}$. If $q = 1$, then $l = 16$, or $L_{cr} = 4$, which also corresponds to numerical results given by Young (1976).

The photon capture cross section for an extreme charged black hole turns out to be considerably smaller than the capture cross section of a Schwarzschild black hole. The critical value of the impact parameter, characterizing the capture cross section for a Reissner - Nordström black hole, is determined by the equation (Zakharov 1991a,b, 1994a)

$$l = \frac{(8q^2 - 36q + 27) + \sqrt{(8q^2 - 36q + 27)^2 + 64q^3(1-q)}}{2(1-q)}. \tag{11}$$

A.F. Zakharov & F. De Paolis, A.A. Nucita, G.Ingrosso, **Astron. & Astrophys., 442, 795 (2005)**

As it was explained by Zakharov et al. (2005a,b) this leads to the formation of shadows described by the critical value of L_{cr} or, in other words, in the spherically symmetric case, shadows are circles with radii L_{cr}. Therefore, measuring the shadow size, one could evaluate the black hole charge in black hole mass units M.

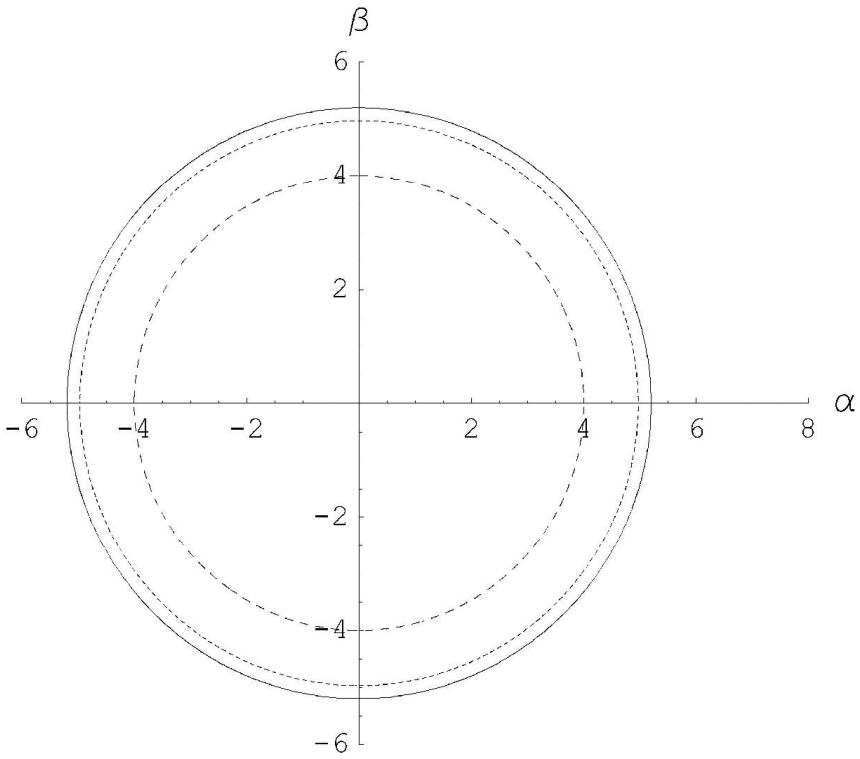

Fig. 1. Shadow (mirage) sizes are shown for selected charges of black holes $Q = 0$ (solid line), $Q = 0.5$ (short dashed line) and $Q = 1$ (long dashed line).

nature Vol 455 | 4 September 2008 | doi:10.1038/nature07245

LETTERS

Event-horizon-scale structure in the supermassive black hole candidate at the Galactic Centre

Sheperd S. Doeleman[1], Jonathan Weintroub[2], Alan E. E. Rogers[1], Richard Plambeck[3], Robert Freund[4], Remo P. J. Tilanus[5,6], Per Friberg[5], Lucy M. Ziurys[4], James M. Moran[2], Brian Corey[1], Ken H. Young[2], Daniel L. Smythe[1], Michael Titus[1], Daniel P. Marrone[7,8], Roger J. Cappallo[1], Douglas C.-J. Bock[9], Geoffrey C. Bower[3], Richard Chamberlin[10], Gary R. Davis[5], Thomas P. Krichbaum[11], James Lamb[12], Holly Maness[3], Arthur E. Niell[1], Alan Roy[11], Peter Strittmatter[4], Daniel Werthimer[13], Alan R. Whitney[1] & David Woody[12]

The cores of most galaxies are thought to harbour supermassive black holes, which power galactic nuclei by converting the gravitational energy of accreting matter into radiation[1]. Sagittarius A* (Sgr A*), the compact source of radio, infrared and X-ray emission at the centre of the Milky Way, is the closest example of this phenomenon, with an estimated black hole mass that is 4,000,000 times that of the Sun[2,3]. A long-standing astronomical goal is to resolve structures in the innermost accretion flow surrounding Sgr A*, where strong gravitational fields will distort the appearance of radiation emitted near the black hole. Radio observations at wavelengths of 3.5 mm and 7 mm have detected intrinsic structure in Sgr A*, but the spatial resolution of observations at these wavelengths is limited by interstellar scattering[4–7]. Here we report observations at a wavelength of 1.3 mm that set a size of 37^{+16}_{-10} microarcseconds on the intrinsic diameter of Sgr A*. This is less than the expected apparent size of the event horizon of the presumed black hole, suggesting that the bulk of Sgr A* emission may not be centred on the black hole, but arises in the surrounding accretion flow.

The proximity of Sgr A* makes the characteristic angular size scale of the Schwarzschild radius ($R_{\rm Sch} = 2GM/c^2$) larger than for any other black hole candidate. At a distance of ~8 kpc (ref. 8), the Sgr A* Schwarzschild radius is 10 μas, or 0.1 astronomical unit (AU). Multi-wavelength monitoring campaigns[9–11] indicate that activity on scales of a few $R_{\rm Sch}$ in Sgr A* is responsible for observed short-term variability and flaring from radio to X-rays, but direct observations of structure on these scales by any astronomical technique has not been possible. Very-long-baseline interferometry (VLBI) at 7 mm and 3.5 mm wavelength shows the intrinsic size of Sgr A* to have a wavelength dependence, which yields an extrapolated size at 1.3 mm of 20–40 μas (refs 6, 7). VLBI images at wavelengths longer than 1.3 mm, however, are dominated by interstellar scattering effects that broaden images of Sgr A*. Our group has been working to extend VLBI arrays to 1.3 mm wavelength, to reduce the effects of interstellar scattering, and to utilize long baselines to increase angular resolution with a goal of studying the structure of Sgr A* on scales commensurate with the putative event horizon of the black hole. Previous pioneering VLBI work at 1.4 mm wavelength uncertainties resulted in a range for the derived size of 50–170 μas (ref. 12).

On 10 and 11 April 2007, we observed Sgr A* at 1.3 mm wavelength with a three-station VLBI array consisting of the Arizona Radio Observatory 10-m Submillimetre Telescope (ARO/SMT) on Mount Graham in Arizona, one 10-m element of the Combined Array for Research in Millimeter-wave Astronomy (CARMA) in Eastern California, and the 15-m James Clerk Maxwell Telescope (JCMT) near the summit of Mauna Kea in Hawaii. A hydrogen maser time standard and high-speed VLBI recording system were installed at both the ARO/SMT and CARMA sites to support the observation. The JCMT partnered with the Submillimetre Array (SMA) on Mauna Kea, which housed the maser and the VLBI recording system and provided a maser-locked receiver reference to the JCMT. Two 480-MHz passbands sampled to two-bit precision were recorded at each site, an aggregate recording rate of 3.84×10^9 bits per second (Gbit s^{-1}). Standard VLBI practice is to search for detections over a range of interferometer delay and delay rate. Six bright quasars were detected with high signal to noise on all three baselines allowing array geometry, instrumental delays and frequency offsets to be accurately calibrated. This calibration greatly reduced the search space for detections of Sgr A*. All data were processed on the Mark4 correlator at the MIT Haystack Observatory in Massachusetts.

On both 10 and 11 April 2007, Sgr A* was robustly detected on the short ARO/SMT–CARMA baseline and the long ARO/SMT–JCMT baseline. On neither day was Sgr A* detected on the CARMA–JCMT baseline, which is attributable to the sensitivity of the CARMA station being about a third that of the ARO/SMT (owing to weather, receiver temperature and aperture efficiency). Table 1 lists the Sgr A* detections on the ARO/SMT–JCMT baseline. The high signal to noise ratio, coupled with the tight grouping of residual delays and delay rates, makes the detections robust and unambiguous.

There are too few visibility measurements to form an image by the usual Fourier transform techniques; hence, we fit models to the visibilities (shown in Fig. 1). We first modelled Sgr A* as a circular Gaussian brightness distribution, for which one expects a Gaussian relationship between correlated flux density and projected baseline length. The weighted least-squares best-fit model (Fig. 1) corre-

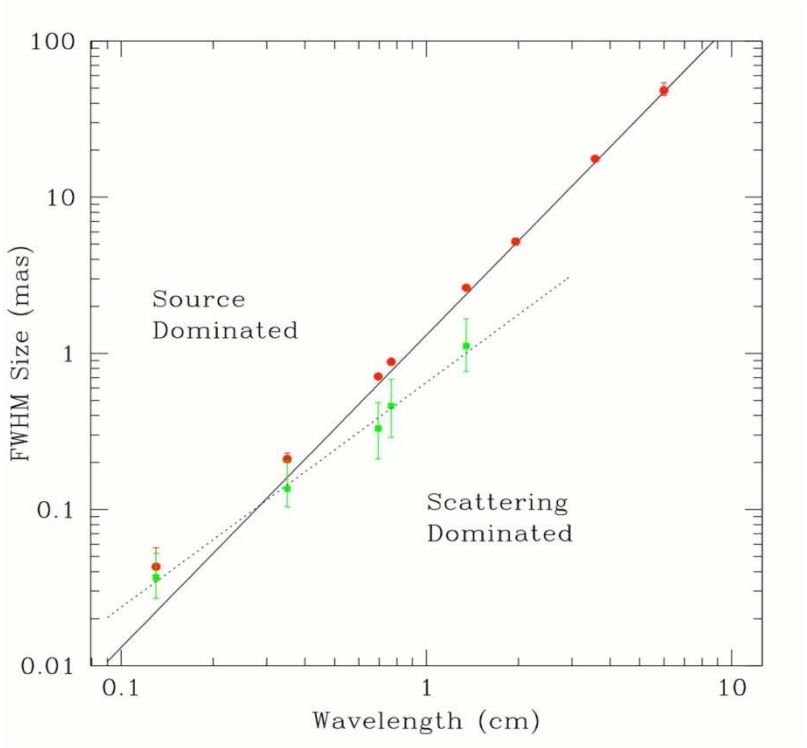

Fig 2

Figure 2 Observed and intrinsic size of Sgr A* as a function of wavelength. Red circles show major-axis observed sizes of Sgr A* from VLBI observations (all errors 3σ). Data from wavelengths of 6 cm to 7 mm are from ref. 13, data at 3.5 mm are from ref. 7, and data at 1.3 mm are from the observations reported here. The solid line is the best-fit λ^2 scattering law from ref. 13, and is derived from measurements made at $\lambda > 17$ cm. Below this line, measurements of the intrinsic size of Sgr A* are dominated by scattering effects, while measurements that fall above the line indicate intrinsic structures that are larger than the scattering size (a 'source-dominated' regime). Green points show derived major-axis intrinsic sizes from 2 cm $< \lambda <$ 1.3 mm and are fitted with a λ^{α} power law ($\alpha = 1.44 \pm 0.07$, 1σ) shown as a dotted line. When the 1.3-mm point is removed from the fit, the power-law exponent becomes $\alpha = 1.56 \pm 0.11$ (1σ).

RADIO INTERFEROMETER MUCH LARGER THE EARTH

"SPECTR-R" (Mission "RadioAstron")

Main scientific tasks of the mission –

syntheses of high-precision images of various Universe objects, its coordinates measurements and search their variability with the time. A fringe width of the system is

up to 7 micro arc seconds.

Main characteristics of the space radio telescope

Spectral band:

- wavelength (cm) - 92; 18; 6.2; 1.19-1.63
- frequency (GHz) - 0.327; 1.66; 4.83; 18-26

Main organizations:

on scientific complex - Astro Space Center of Lebedev Physical Institute of Russian Academy of Science;

of spacecraft - Lavochkin Research Production Association of Russian Space Agency.

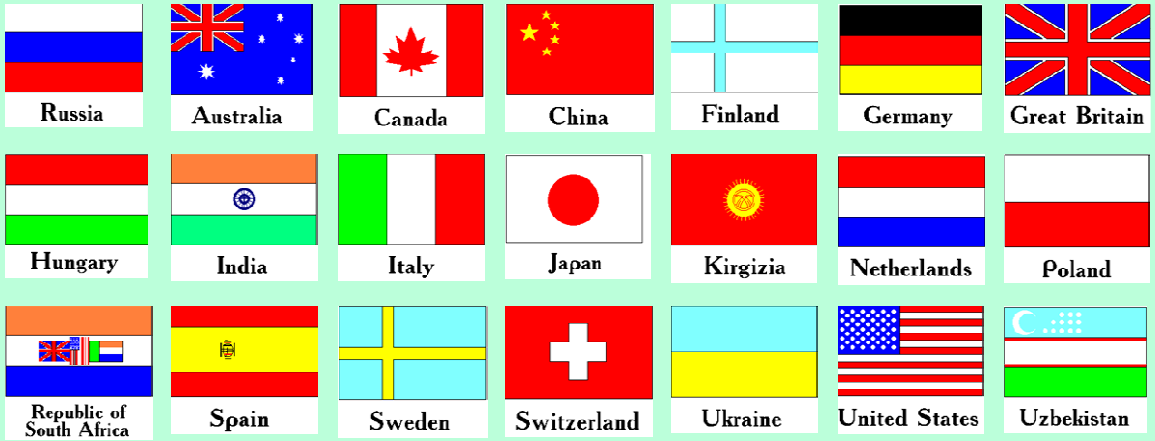

Planned launch date of the mission is 2007.

The orbit of the mission :

apogee -	310 000 - 370 000 km
perigee -	10 000 - 70 000 km
declination -	51.6 °
period variation -	7 - 10 days
Guarantied time of activity -	5 years
Scientific payload mass -	2100 kg
Pointing accuracy of radio telescope -	35"

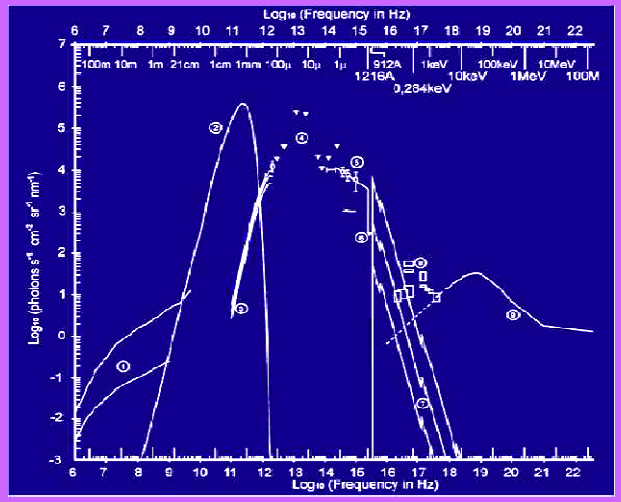

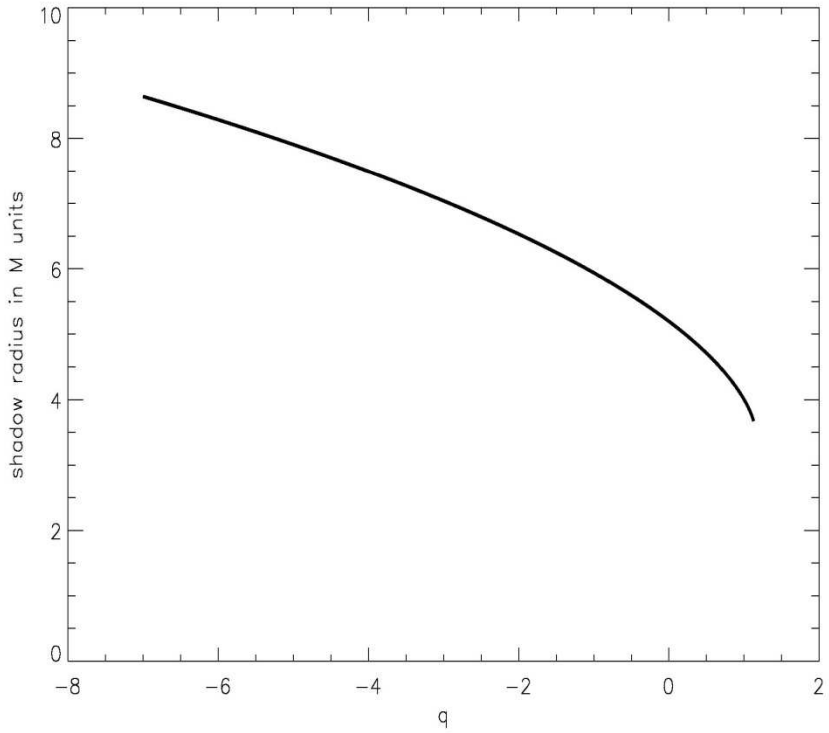
10
8
6
4
2
0
shadow radius in M units
−8
−6
−4
−2
0
2
q

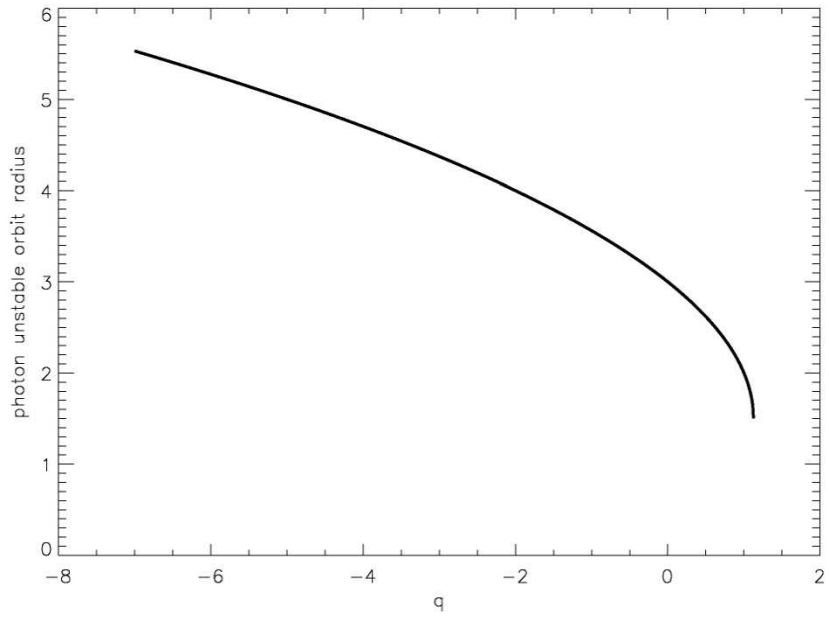
photon unstable orbit radius
q
0
1
2
3
4
5
6
−8
−6
−4
−2
0
2

Recently,Bin-Nun (2010) discussed an opportunity that the black hole at the Galactic Center is described by the tidal Reissner-- Nordstrom metric which may be admitted by the Randall--Sundrum II braneworld scenario. Bin-Nun suggested an opportunity of evaluating the black hole metric analyzing (retro-)lensing of bright stars around the black hole in the Galactic Center. Doeleman et al. (2008) evaluated a shadow size for the black hole at the Galactic Center. Measurements of the shadow size around the black hole may help to evaluate parameters of black hole metric Zakharov et al (2005). We derive an analytic expression for the black hole shadow size as a function of charge for the tidal Reissner-- Nordstrom metric. We conclude that observational data concerning shadow size measurements are not consistent with significant negative charges, in particular, the significant negative charge $Q/(4M^2)=-1.6$ (discussed by Bin-Nun (2010) is practically ruled out with a very probability (the charge is roughly speaking is beyond 9 σ confidence level, but a negative charge is beyond 3 σ confidence level).

RADIO INTERFEROMETER MUCH LARGER THE EARTH

"SPECTR-R" (Mission "RadioAstron")

Main scientific tasks of the mission –

syntheses of high-precision images of various Universe objects, its coordinates measurements and search their variability with the time. A fringe width of the system is

up to 7 micro arc seconds.

Main characteristics of the space radio telescope

Spectral band:

- wavelength (cm) - 92; 18; 6.2; 1.19-1.63
- frequency (GHz) - 0.327; 1.66; 4.83; 18-26

Main organizations:

on scientific complex - Astro Space Center of Lebedev Physical Institute of Russian Academy of Science;

of spacecraft - Lavochkin Research Production Association of Russian Space Agency.

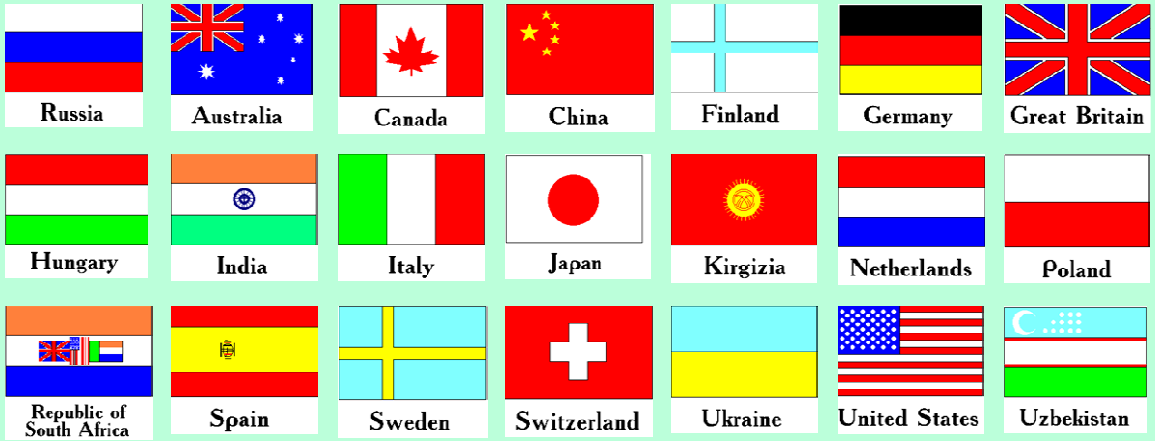

Planned launch date of the mission is 2007.

The orbit of the mission :

apogee -	310 000 - 370 000 km
perigee -	10 000 - 70 000 km
declination -	51.6 °
period variation -	7 - 10 days
Guarantied time of activity -	5 years
Scientific payload mass -	2100 kg
Pointing accuracy of radio telescope -	35"

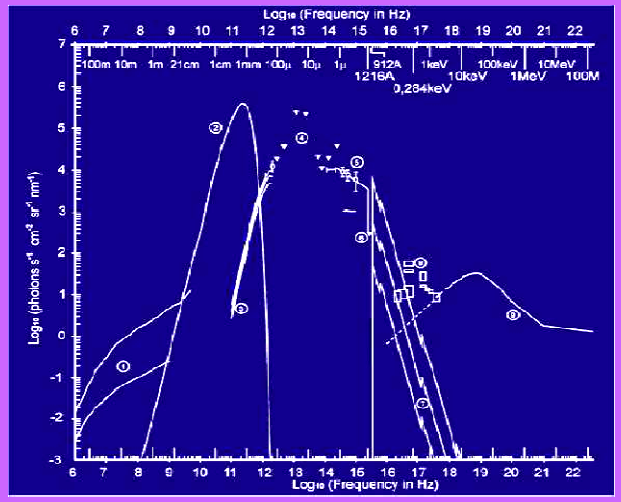

XMM-Newton observations of MCG-6-30-15 in the 2-10 keV band

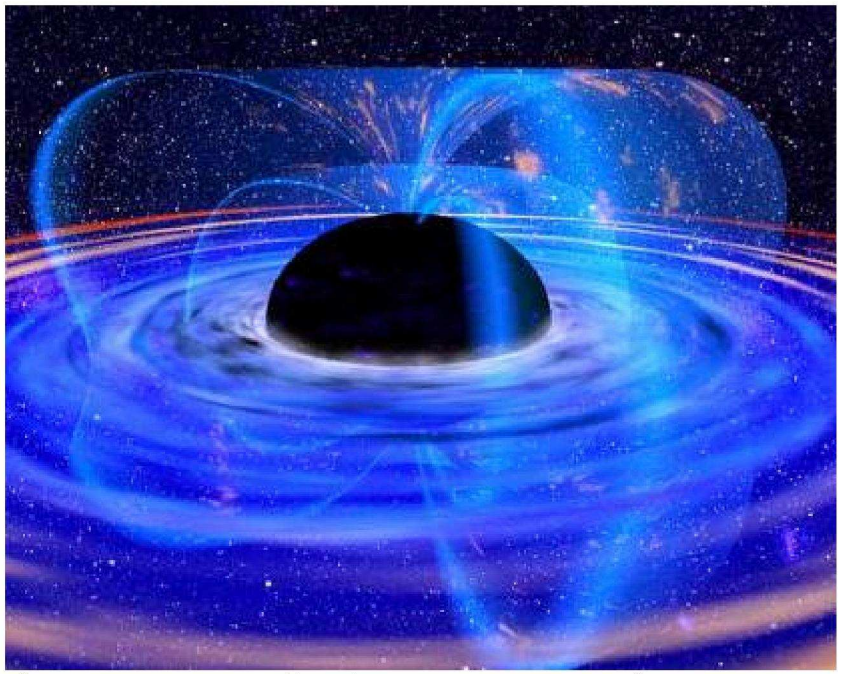

Wilms et al 2002; Fabian et al 2002; Vaughan et al 2002; Fabian & Vaughan 2002; Ballantyne et al 2003; Reynolds et al 2003; Vaughan & Fabian 2004

Understanding the spectral behaviour

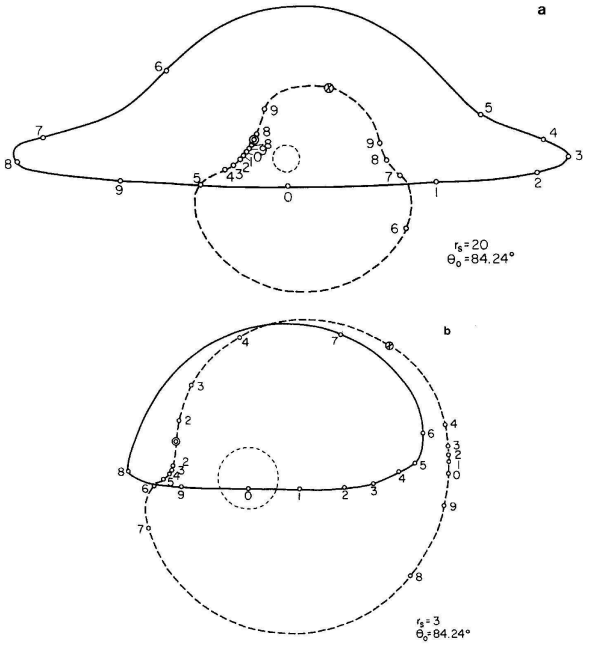

FIG. 8.—Apparent positions of the two brightest images as functions of time for two orbital radii and an observer at a polar angle $\theta_0 = 84°24$. The small, dashed circle in each plot is the locus $\alpha^2 + \beta^2 = 1$ and gives the scale of the plot. The direct image moves along the solid line; the one-orbit image, along the dashed line. Ticks mark the positions of the images at 10 equally spaced times. A pair of one-orbit images appears to be created at the points ⊙ and annihilated at the points ⊗. See text.

fore of α) and the variation in surface brightness increase more rapidly for the one-orbit image than for the direct image as we consider stars of progressively smaller orbital radii.

As the apparent position of the image seen by the distant observer changes, so does the corresponding direction of emission in the local rest frame of the star. If the instantaneous direction of emission of the beam of radiation which reaches the observer is represented by a point in figure 3 (for $r_s = 1.5$), this point moves along the $\cos \theta_0 =$ const. curve corresponding to the given type of image in the direction indicated by the arrows. Creation of pairs of images on the one-orbit curves is at the points marked ◎; destruction, at points ⊗. For $r_s = 1.5$ there is no retrograde image and, hence, no creation and destruction of images for observers with $\theta_0 \lesssim 40°$.

When r_s is not much larger than unity, the images move very slowly on the parts of the curves nearest the backward ϕ-direction and very rapidly on the remainder of the

Schwarzschild black hole images (P. Jovanovic , L.C. Popovic & A.F.Z. in preparation)

θ=15 deg

- Redshift map

Intensity map

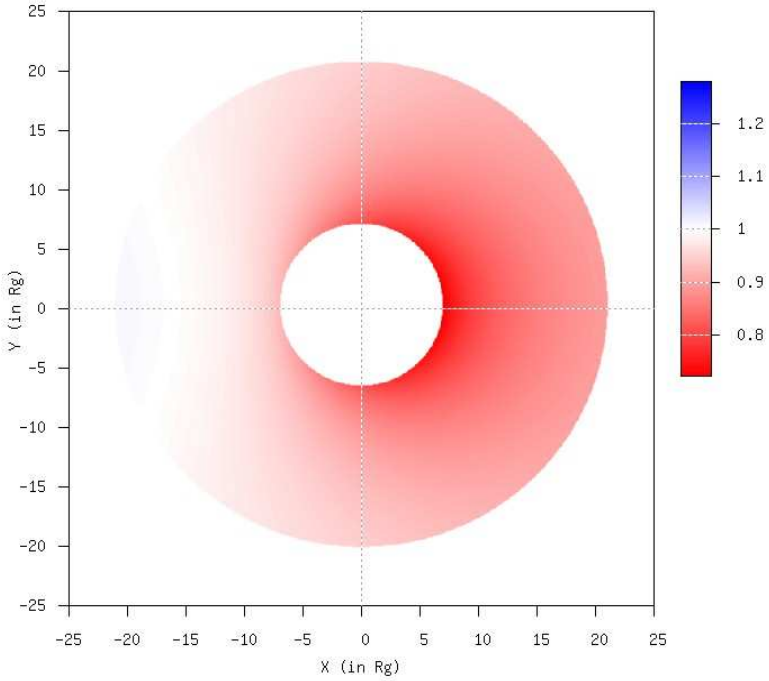

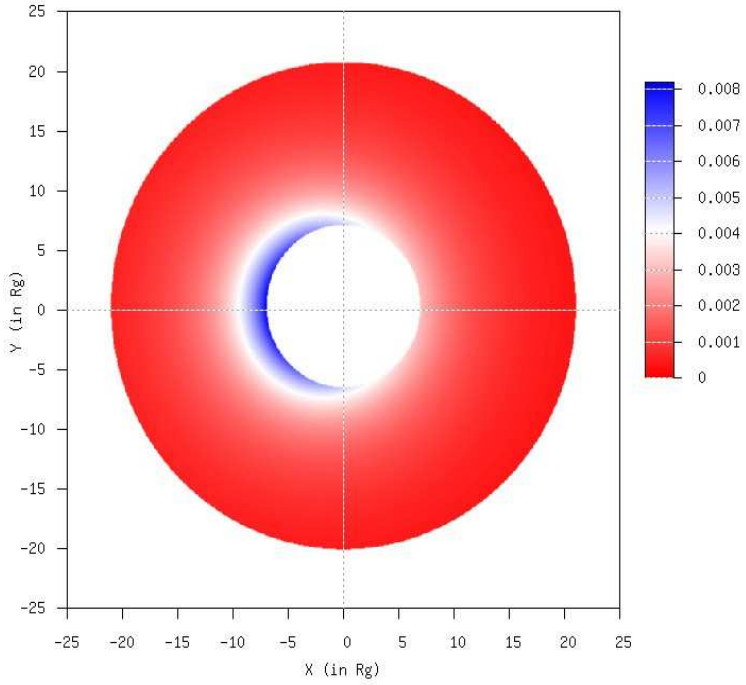

Schwarzschild black hole images: θ=85 deg

- Redshift map
- Intensity map

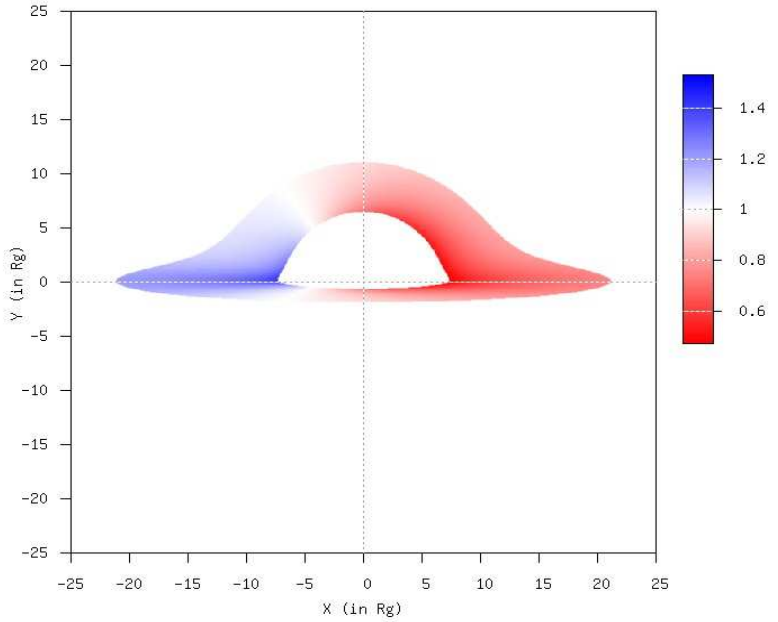

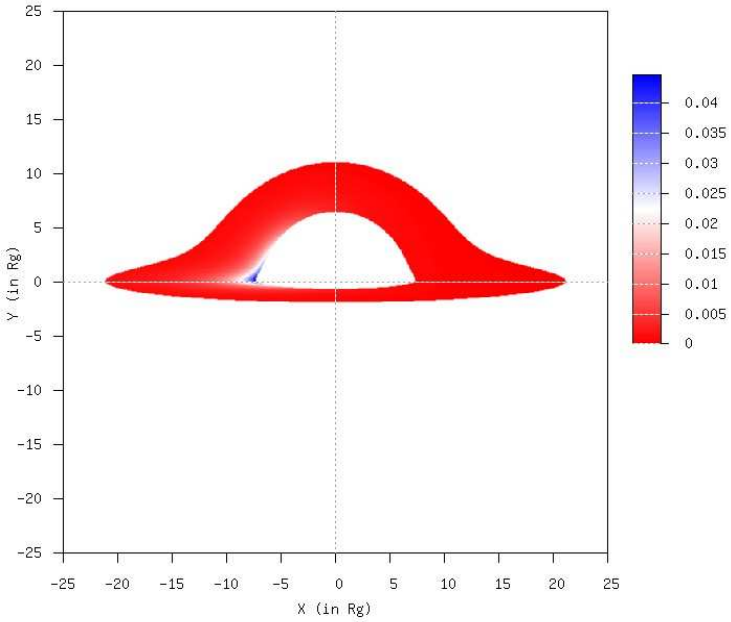

Kerr black hole images (a=0.75): **θ=85 deg**

- Redshift map

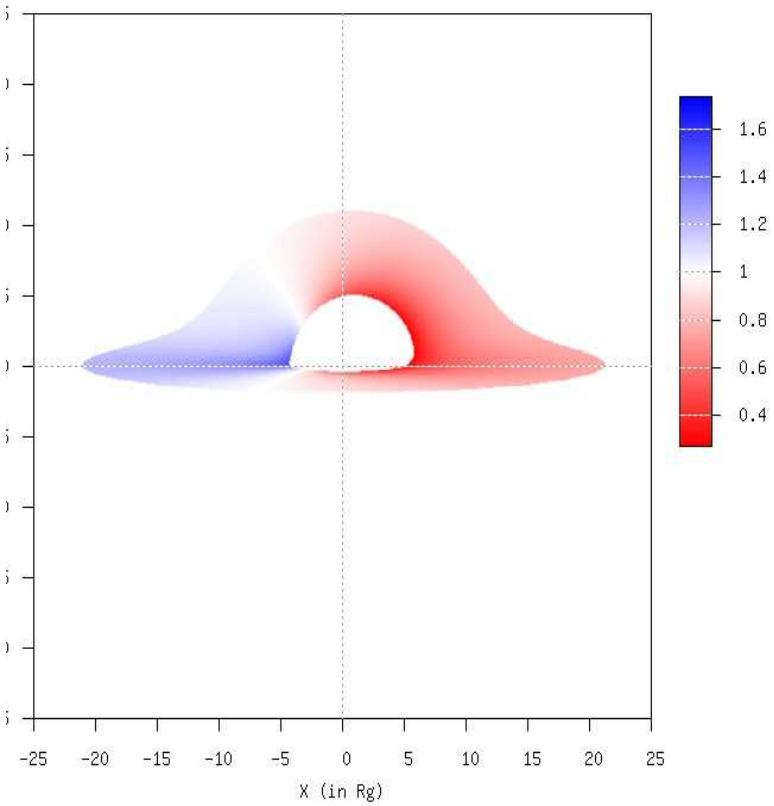

- Intensity map

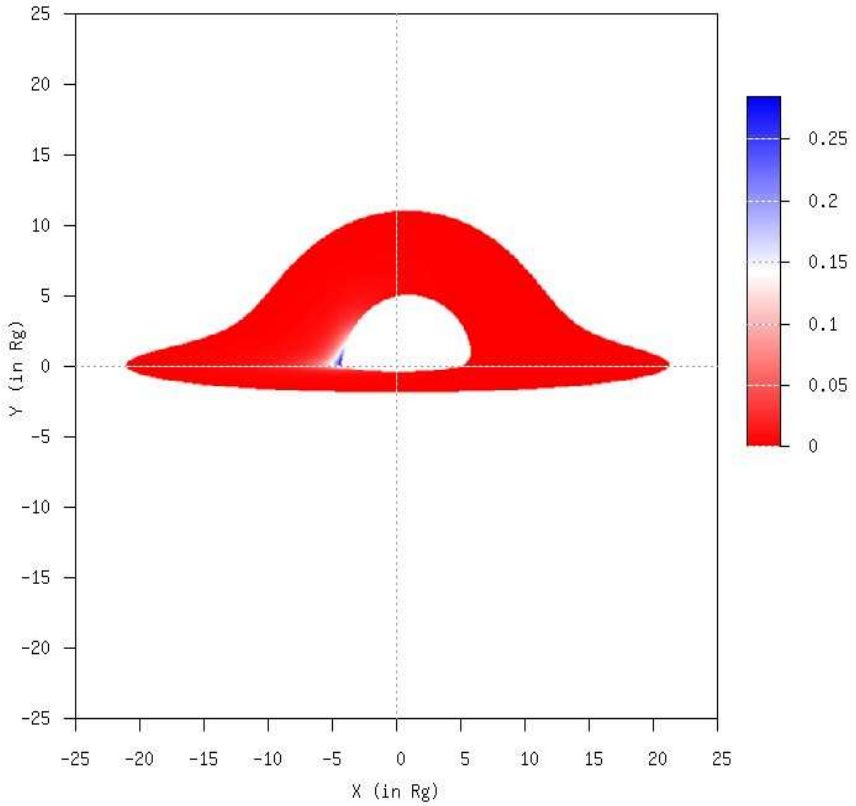

Kerr black hole images (a=0.99): **θ=85 deg**

- Redshift map

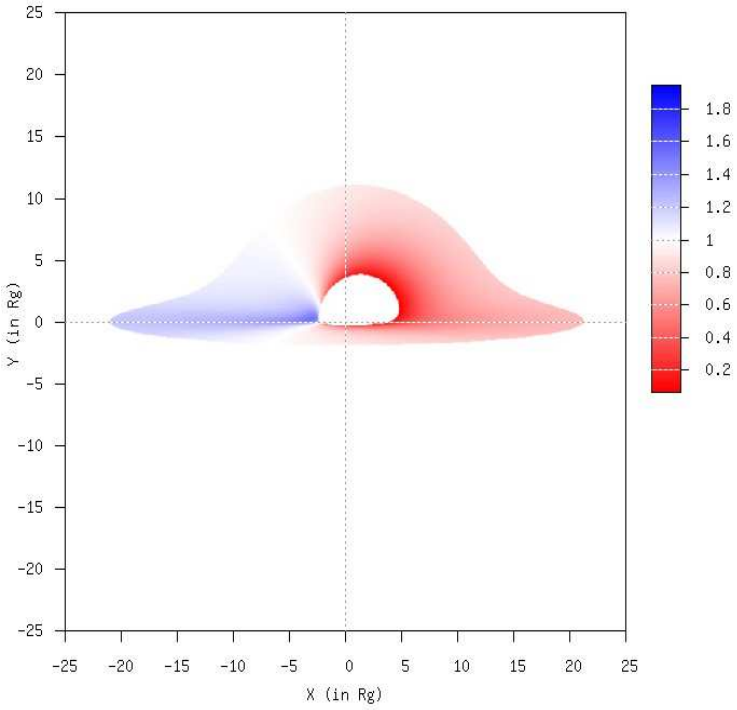

- Intensity map

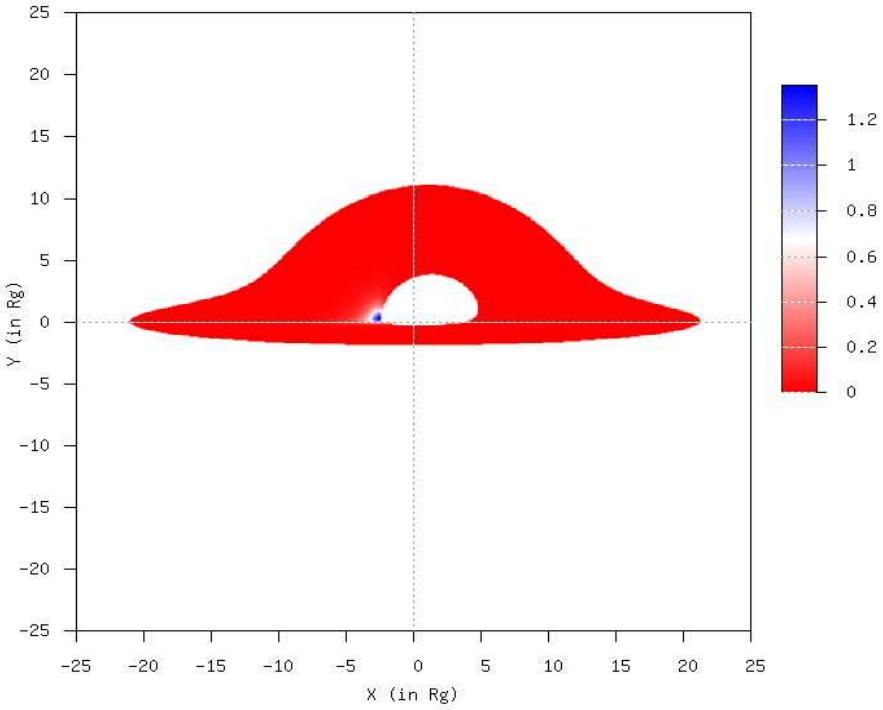

Falcke, Melia, Agol

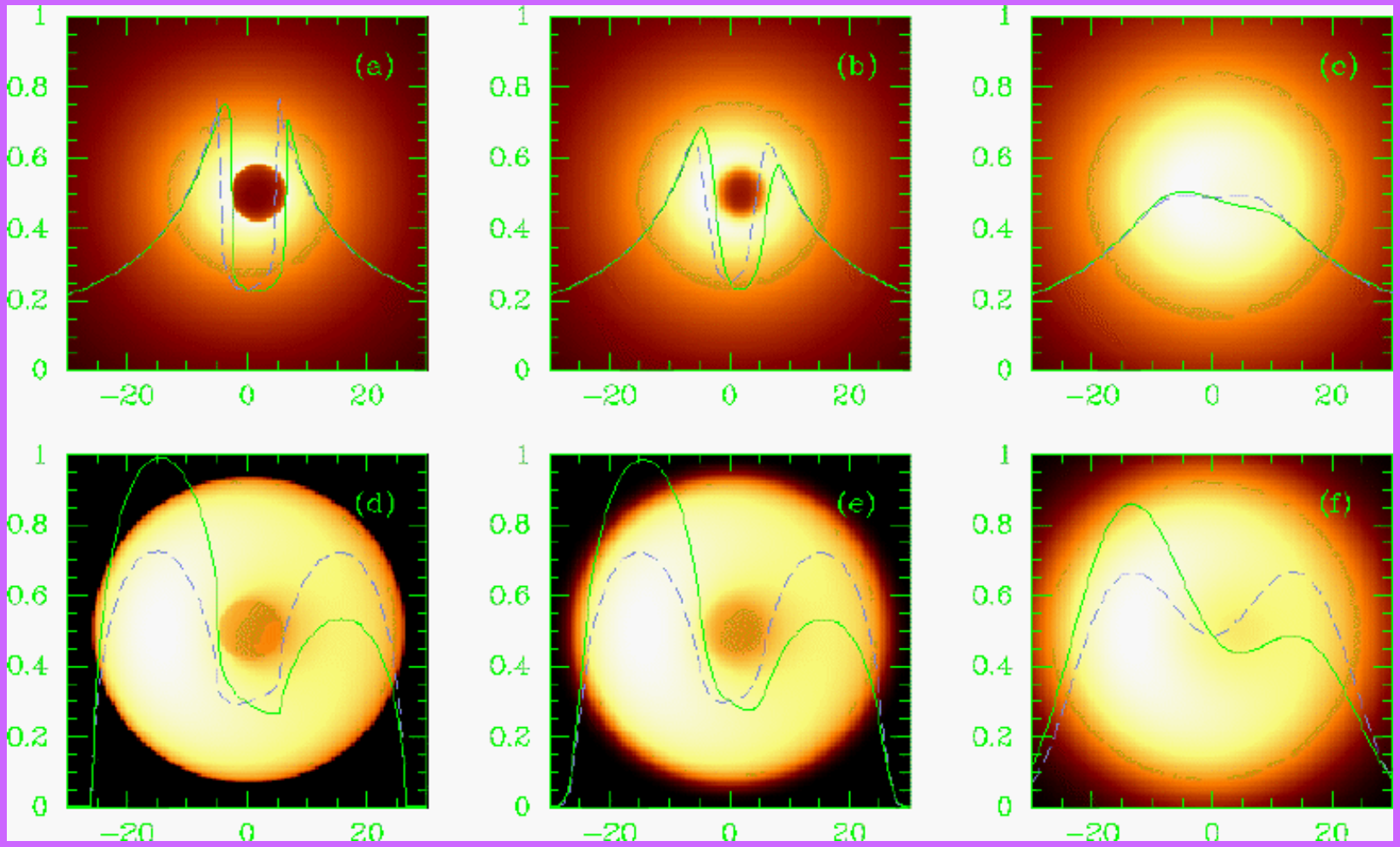

Shadows from Melia

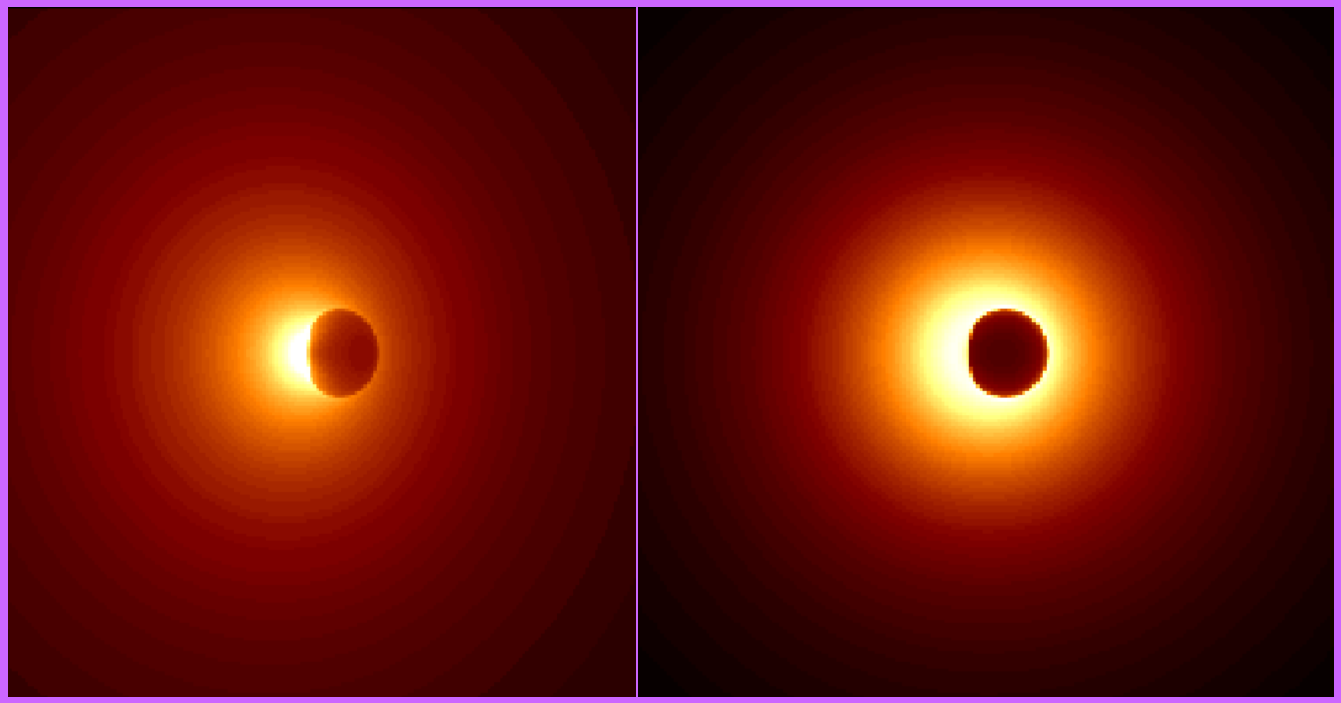

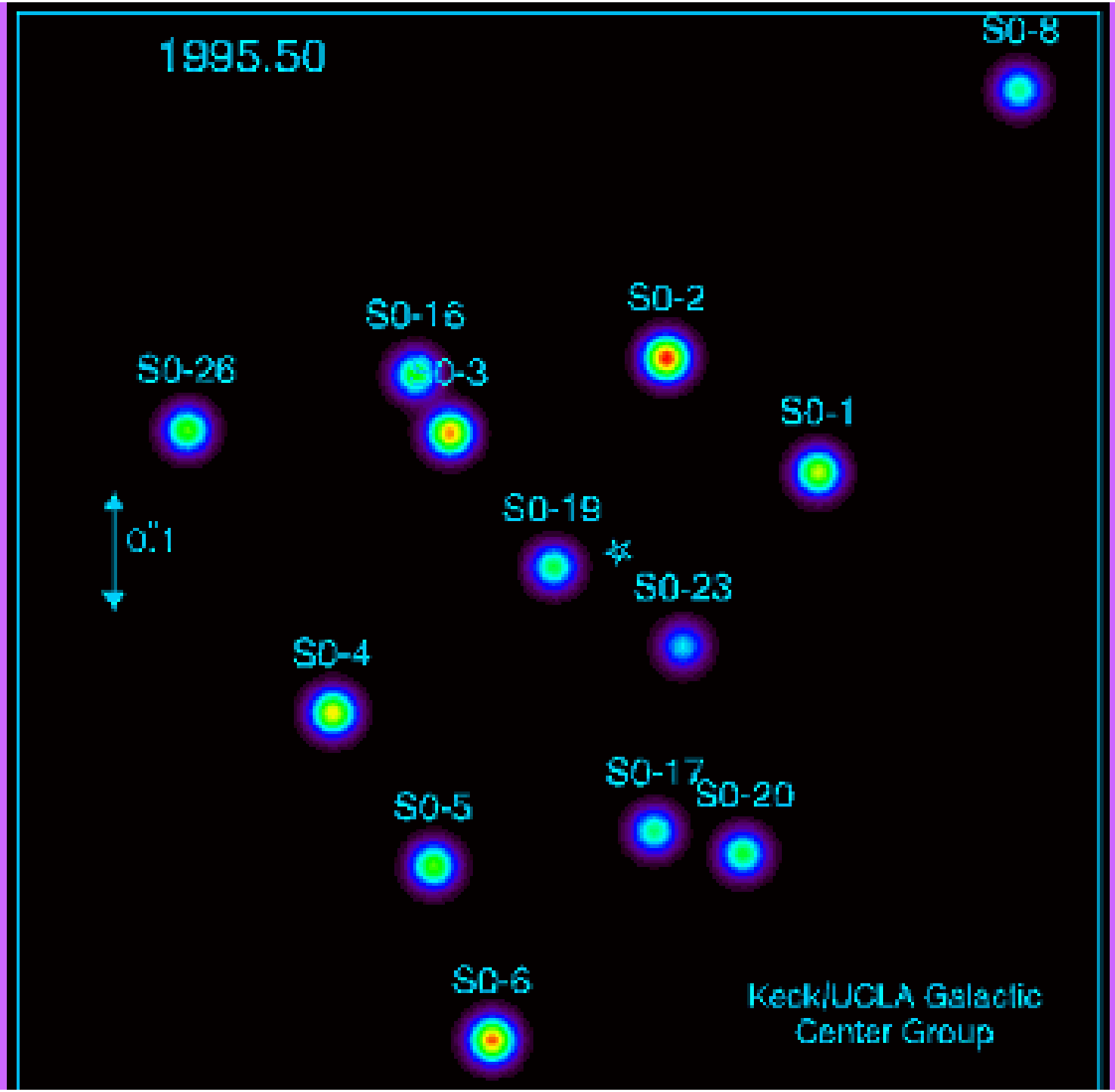
1995.50
S0-8
S0-16
S0-2
S0-26
S0-3
S0-1
0.1
S0-19
S0-23
S0-4
S0-17
S0-20
S0-5
S0-6
Keck/UCLA Galactic
Center Group

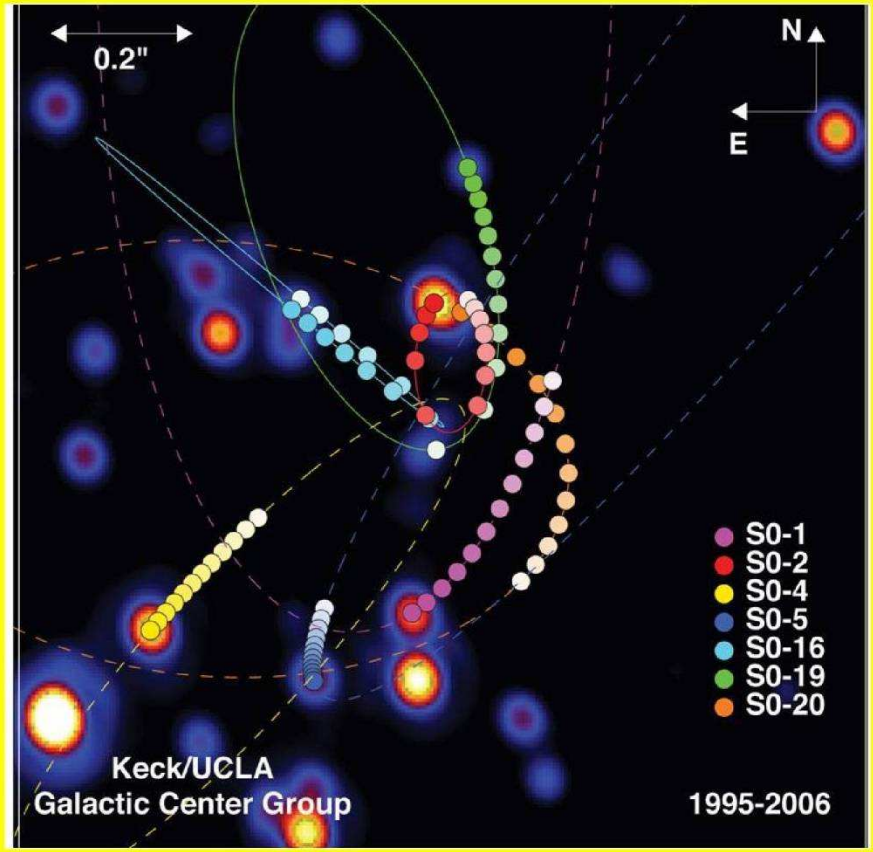

Figure 19: Bright stars near the Galactic Centre.

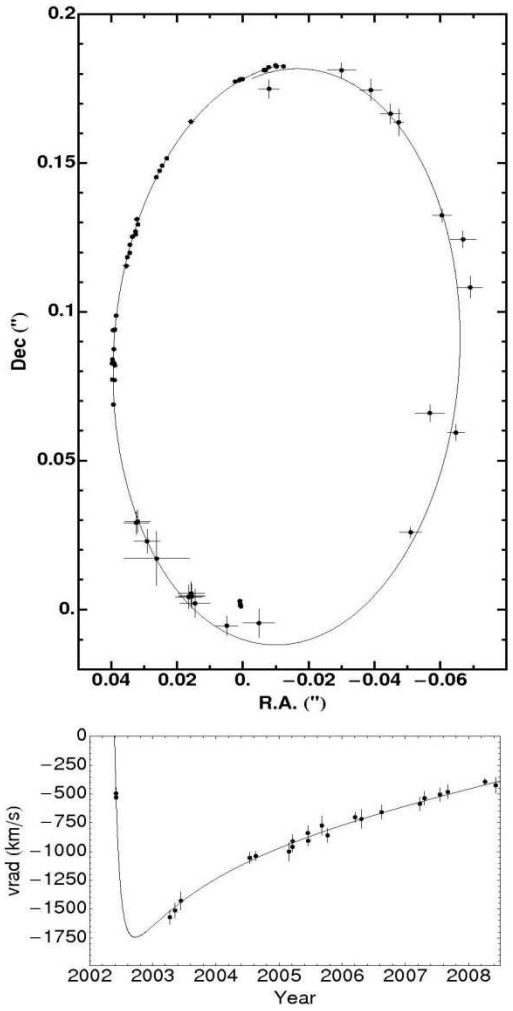

FIG. 13.— Top: The S2 orbital data plotted in the combined coordinate system and fitted with a Keplerian model in which the velocity of the central point mass and its position were free fit parameters. The non-zero velocity of the central point mass is the reason why the orbit figure does not close exactly in the overlap region 1992/2008 close to apocenter. The fitted position of the central point mass is indicated by the elongated dot inside the orbit near the origin; its shape is determined from the uncertainty in the position and the fitted velocity, which leads to the elongation. Bottom: The measured radial velocities of S2 and the radial velocity as calculated from the orbit fit.

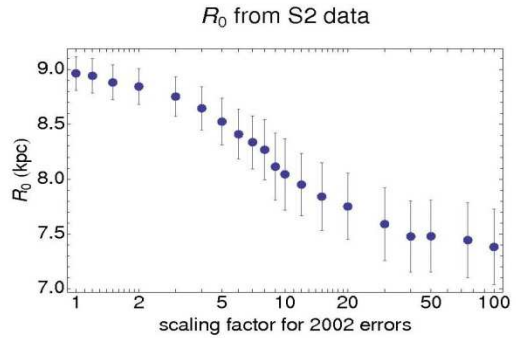

FIG. 14.— Fitted value of R_0 for various scaling factors of the S2 2002 data, using a fit with the coordinate system priors. The factor by which the 2002 astrometric errors of the S2 data is scaled up strongly influences the distance. The mean factor determined in Figure 9 is ≈ 7, corresponding to $R_0 \approx 8.1$kpc.

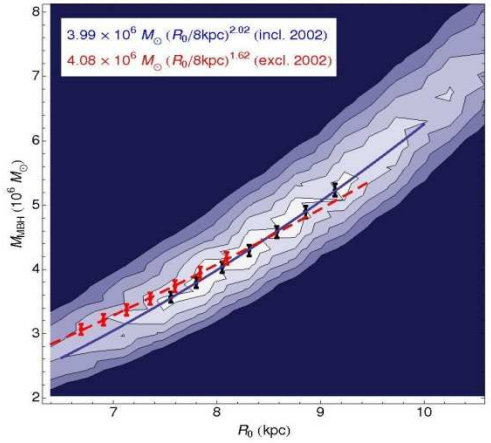

FIG. 15.— Contour plot of χ^2 as function of R_0 and central point mass. The two parameters are strongly correlated. The contours are generated from the S2 data including the 2002 data; fitting at each point all other parameters both of the potential and the orbital elements. The black dots indicate the position and errors of the best fit values of the mass for the respective distance; the blue line is a power law fit to these points; the corresponding function is given in the upper row of the text box. The central point is chosen at the best fitting distance. The red points and the red dashed line are the respective data and fit for the S2 data excluding the 2002 data; the fit is reported in the lower row of the text box. The contour levels are drawn at confidence levels corresponding to 1σ, 3σ, 5σ, 7σ, 9σ.

From the numbers it seems that the fit excluding the

An Expanded View of the Universe

Science with the
European Extremely Large Telescope

Black Holes

Black holes are some of the most bizarre objects in the Universe, challenging the imaginations of even the most creative scientists. They are places where gravity trumps all other forces in the Universe, pushing our understanding of physics to the limit. Even more strangely, supermassive black holes seem to play a key role in the formation of galaxies and structures in the Universe.

Galactic Centre

Over the last 15 years or so, an enormous amount of work has gone into improving our understanding of the closest supermassive black hole — Sagittarius A* at the centre of the Milky Way.

Technological progress, in particular in the areas of adaptive optics and high angular resolution with ground-based 8-metre-class telescopes, has allowed impressive progress in understanding supermassive black holes and their surroundings. Key progress was made in proving the very existence of a supermassive black hole at the centre of the Milky Way, in refining our knowledge of how matter falls into black holes, and in identifying gas discs and young stars in the immediate vicinity of the black hole. The Galactic Centre was thus established as the most important laboratory for the study of supermassive black holes and their surroundings.

But its potential for progress in fundamental physics and astrophysics is far from being fully exploited. The Galactic Centre remains the best place to test general relativity directly in a strong gravitational field. The E-ELT will enable extremely accurate measurements of the positions of stars (at the 50–100 microarcsecond level over fields of tens of arcseconds), as well as radial velocity measurements with about 1 km/s precision, pushing our observations ever closer to the black hole event horizon. Stars can then be discovered at 100 Schwarzschild radii, where orbital velocities approach a tenth of the speed of light. This is more than ten times closer than can be achieved with the current generation of telescopes. Such stellar probes will allow us to test the predicted relativistic signals of black hole spin and the gravitational redshift caused by the black hole, and even to detect gravitational wave effects. Further out, the dark matter distribution around the black hole, predicted by cold dark matter cosmologies (ΛCDM), can be explored. The distance to the Galactic Centre can be measured to 0.1%, constraining in turn the size and shape of the galactic halo and the Galaxy's local rotation speed to unprecedented levels. Crucial progress in our understanding of the interaction of the black hole with its surroundings will be made. The puzzling stellar cusp around the Galactic Centre, as well as the observed star formation in the vicinity of the black hole will be studied in detail for the first time.

Left: Very Large Telescope (VLT) observations have revealed that the supermassive black hole closest to us is located in the centre of the Milky Way.

The Milky Way's central supermassive black hole has been weighed by measuring the proper motions of stars in its vicinity.

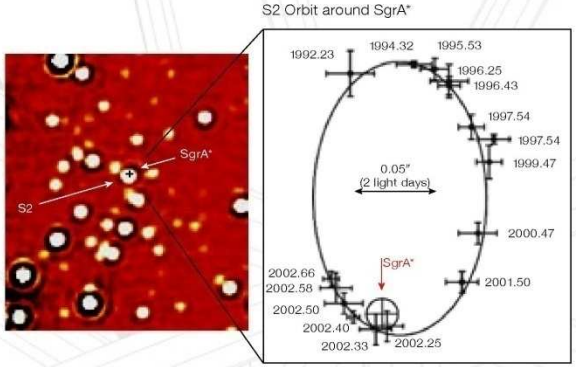

GRAVITY

Studying the supermassive black hole at the center of the Galaxy

46th Rencontres de Moriond and GPHyS colloquium 2011
Gravitational Waves and Experimental Gravity

Guy Perrin and the GRAVITY consortium

l'Observatoire de Paris | LESIA
Laboratoire d'Études Spatiales et d'Instrumentation en Astrophysique

Thursday 25 March 2011

The VLT, *Very Large Telescope*
4 european 8 m telescopes at Cerro Paranal in Chili

Going beyond boundaries thanks to accurate spatial information

- Bring the ultimate evidence that Sgr A* is a black hole: the mass is contained in the Schwarzschild radius.
- Understand the nature of flares.
- Use the black hole as a tool to study general relativity in the strong field regime

Scale ~ 1 R_s 10 µas

- Study relativistic effects on nearby stars
- Understand the nature of S stars and their distribution

Scale ~ 100 R_s 1 mas

For a test particle orbiting a Schwarzschild black hole of mass $M_{\rm BH}$, the periastron shift is given by (see e.g. Weinberg, 1972)

$$\Delta\phi_S \simeq \frac{6\pi G M_{BH}}{d(1-e^2)c^2} + \frac{3(18+e^2)\pi G^2 M_{BH}^2}{2d^2(1-e^2)^2c^4} \ , \qquad (9)$$

d and e being the semi-major axis and eccentricity of the test particle orbit, respectively. For a rotating black hole with spin parameter $a = |\mathbf{a}| = J/GM_{\rm BH}$, the space-time is described by the Kerr metric and, in the most favorable case of equatorial plane motion (**(a,v)** $= 0$), the shift is given by (Boyer and Price (1965))

$$\Delta\phi_K \simeq \Delta\phi_S + \frac{8a\pi M_{BH}^{1/2} G^{3/2}}{d^{3/2}(1-e^2)^{3/2}c^3} + \frac{3a^2\pi G^2}{d^2(1-e^2)^2c^4} \ , \qquad (10)$$

which reduces to eq. (9) for $a \to 0$. In the more general case, **a.v** $\neq 0$, the

expected periastron shift has to be evaluated numerically.

The expected periastron shifts (mas/revolution), $\Delta\phi$ (as seen from the center) and $\Delta\phi_E$ (as seen from Earth at the distance $R_0 \simeq 8$ kpc from the GC), for the Schwarzschild and the extreme Kerr black holes, for the S2 and S16 stars turn out to be $\Delta\phi^{S2} = 6.3329 \times 10^5$ and 6.4410×10^5 and $\Delta\phi_E^{S2} = 0.661$ and 0.672 respectively, and $\Delta\phi^{S16} = 1.6428 \times 10^6$ and 1.6881×10^6 and $\Delta\phi_E^{S16} = 3.307$ and 3.399 respectively. Recall that

$$\Delta\phi_E = \frac{d(1+e)}{R_0}\Delta\phi_{S,K} \ . \tag{11}$$

Notice that the differences between the periastron shifts for the Schwarzschild and the maximally rotating Kerr black hole is at most 0.01 mas for the S2 star and 0.009 mas for the S16 star. In order to make these measurements with the required accuracy, one needs to know the S2 orbit with a precision of at least 10 μas.

The star cluster surrounding the central black hole in the GC could be sizable. At least 17 members have been observed within 15 mpc up to now (Ghez et al. (2005)). However, the cluster mass and density distribution, that is to say its mass and core radius, is still unknown. The presence of this cluster affects the periastron shift of stars orbiting the central black hole. The periastron advance depends strongly on the mass density profile and especially on the central density and typical length scale.

We model the stellar cluster by a Plummer model density profile (Binney & Tremaine (1987))

$$\rho_{CL}(r) = \rho_0 f(r) \ , \qquad \text{with} \qquad f(r) = \left[1 + \left(\frac{r}{r_c}\right)^2\right]^{-\alpha/2} \ , \quad (12)$$

and the mass contained within r is

$$M(r) = \lambda_{BH} M + \int_0^r 4\pi r'^2 \rho_0 f(r') \, dr' \ . \tag{15}$$

According to GR, the motion of a test particle can be fully described by solving the geodesic equations. Under the assumption that the matter distribution is static and pressureless, the equation of motion of the test particle becomes (see e.g. Weinberg 1972))

$$\frac{d\mathbf{v}}{dt} \simeq -\nabla(\Phi_N + 2\Phi_N^2) + 4\mathbf{v}(\mathbf{v}\cdot\nabla)\Phi_N - v^2\nabla\Phi_N \ . \tag{16}$$

For the S2 star, d and e given in the literature are 919 AU and 0.87 respectively. They yield the orbits of the S2 star for different values of the

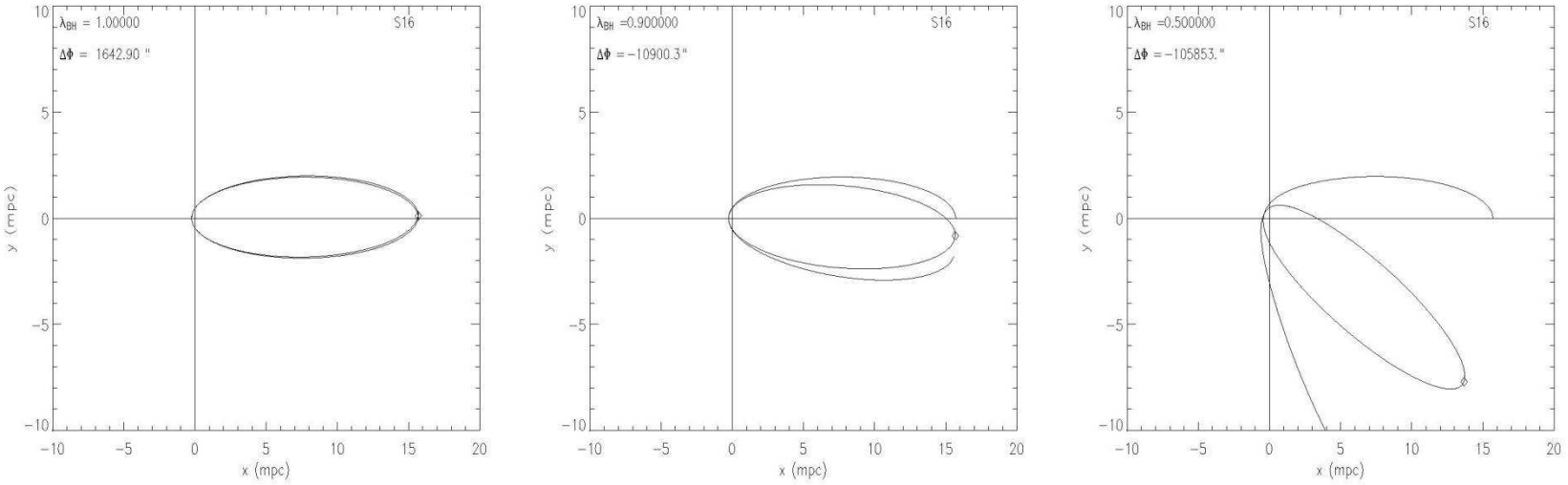

Figure 21: The same as in Figure 20 but for the S16–Sgr A* binary system. In this case, the binary system orbital parameters were taken from Ghez et al. (2005) assuming for the S16 mass a conservative value of $\simeq 10$ $M_\odot$.

AFZ, A.A. Nucita, F. De Paolis, G. Ingrosso, PRD 76, 062001 (2007)

The mass concentration at the Galactic Center

Recent advancements in infrared astronomy are allowing to test the scale of the mass profile at the center of our galaxy down to tens of AU. With the Keck 10 m telescope, the proper motion of several stars orbiting the Galactic Center black hole have been monitored and almost entire orbits, as for example that of the S2 star, have been measured allowing an unprecedent description of the Galactic Center region. Measurements of the amount of mass $M(< r)$ contained within a distance r from the Galactic Center are continuously improved as more precise data are collected. Recent observations (Ghez et al. (2003)) extend down to the periastron distance ($\simeq 3 \times 10^{-4}$ pc) of the S16 star and they correspond to a value of the enclosed mass within $\simeq 3 \times 10^{-4}$ pc of $\simeq 3.67 \times 10^{6}$ $M_{\odot}$. Several authors have used these observations to model the Galactic Center mass concentration. Here and in the following, we use the three component

model for the central region of our galaxy based on estimates of enclosed mass given by Ghez et al (2003, 2005) recently proposed by Hall and Gondolo (2006). This model is constituted by the central black hole, the central stellar cluster and the DM sphere (made of WIMPs), i.e.

$$M(<r) = M_{BH} + M_*(<r) + M_{DM}(<r) \ , \tag{17}$$

where M_{BH} is the mass of the central black hole Sagittarius A*. For the central stellar cluster, the empirical mass profile is

$$M_*(<r) = \begin{cases} M_* \left(\frac{r}{R_*}\right)^{1.6} \ , & r \leq R_* \\ \\ M_* \left(\frac{r}{R_*}\right)^{1.0} \ , & r > R_* \end{cases} \tag{18}$$

with a total stellar mass $M_* = 0.88 \times 10^6$ M$_\odot$ and a size $R_* = 0.3878$ pc.

As far as the mass profile of the DM concentration is concerned, Hall & Gondolo (2006) have assumed a mass distribution of the form

$$M_{DM}(<r) = \begin{cases} M_{DM}\left(\frac{r}{R_{DM}}\right)^{3-\alpha}, & r \leq R_{DM} \\ M_{DM}, & r > R_{DM} \end{cases} \quad (19)$$

M_{DM} and R_{DM} being the total amount of DM in the form of WIMPs and the radius of the spherical mass distribution, respectively.

Hall and Gondolo (2006) discussed limits on DM mass around the black hole at the Galactic Center. It is clear that present observations of stars around the Galactic Center do not exclude the existence of a DM sphere with mass $\simeq 4 \times 10^6 M_\odot$, well contained within the orbits of the known stars, if its radius R_{DM} is $\lesssim 2 \times 10^{-4}$ pc (the periastron distance of the S16 star in the more recent analysis (Ghez et al. 2005)). However, if one

Apoastron Shift Constraints

According to GR, the motion of a test particle can be fully described by solving the geodesic equations. Under the assumption that the matter distribution is static and pressureless, the equations of motion at the first post-Newtonian (PN) approximation become (see e.g. (Fock 1961, Weinberg 1972, Rubilar & Eckart 2001))

$$\frac{d\mathbf{v}}{dt} \simeq -\nabla(\Phi_N + 2\Phi_N^2) + 4\mathbf{v}(\mathbf{v}\cdot\nabla)\Phi_N - v^2\nabla\Phi_N \ . \qquad (21)$$

We note that the PN-approximation is the first relativistic correction from which the apoastron advance phenomenon arises. In the case of the S2 star, the apoastron shift as seen from Earth (from Eq. (23)) due to the presence of a central black hole is about 1 mas, therefore not directly

obtained by the black hole only, the black hole plus the stellar cluster and the contribution of two different DM mass density profiles. In each case the S2 orbit apoastron shift is given. As one can see, for selected parameters for DM and stellar cluster masses and radii the effect of the stellar cluster is almost negligible while the effect of the DM distribution is crucial since it enormously overcome the shift due to the relativistic precession. Moreover, as expected, its contribution is opposite in sign with respect to that of the black hole (Nucita et al. (2007)).

We note that the expected apoastron (or, equivalently, periastron) shifts (mas/revolution), $\Delta\Phi$ (as seen from the center) and the corresponding values $\Delta\phi_E^{\pm}$ as seen from Earth (at the distance $R_0 \simeq 8$ kpc from the GC) are related by

$$\Delta\phi_E^{\pm} = \frac{d(1 \pm e)}{R_0}\Delta\Phi, \tag{23}$$

where with the sign $\pm$ are indicated the shift angles of the apoastron $(+)$

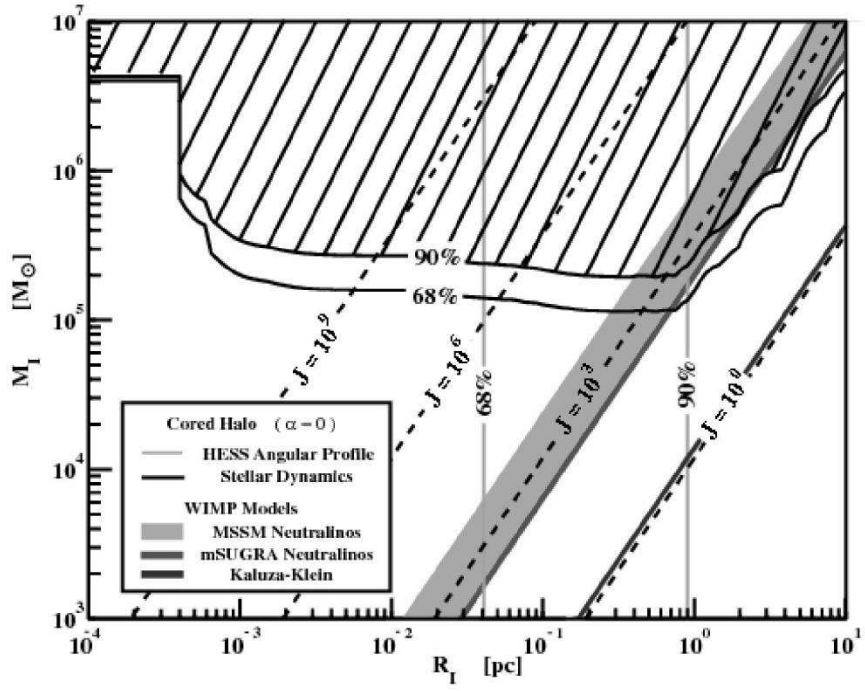

Figure 28: An allowed region for DM distribution from S2 like star trajectories near the Black Hole at the Galactic Center (Hall and Gondolo (2006)).

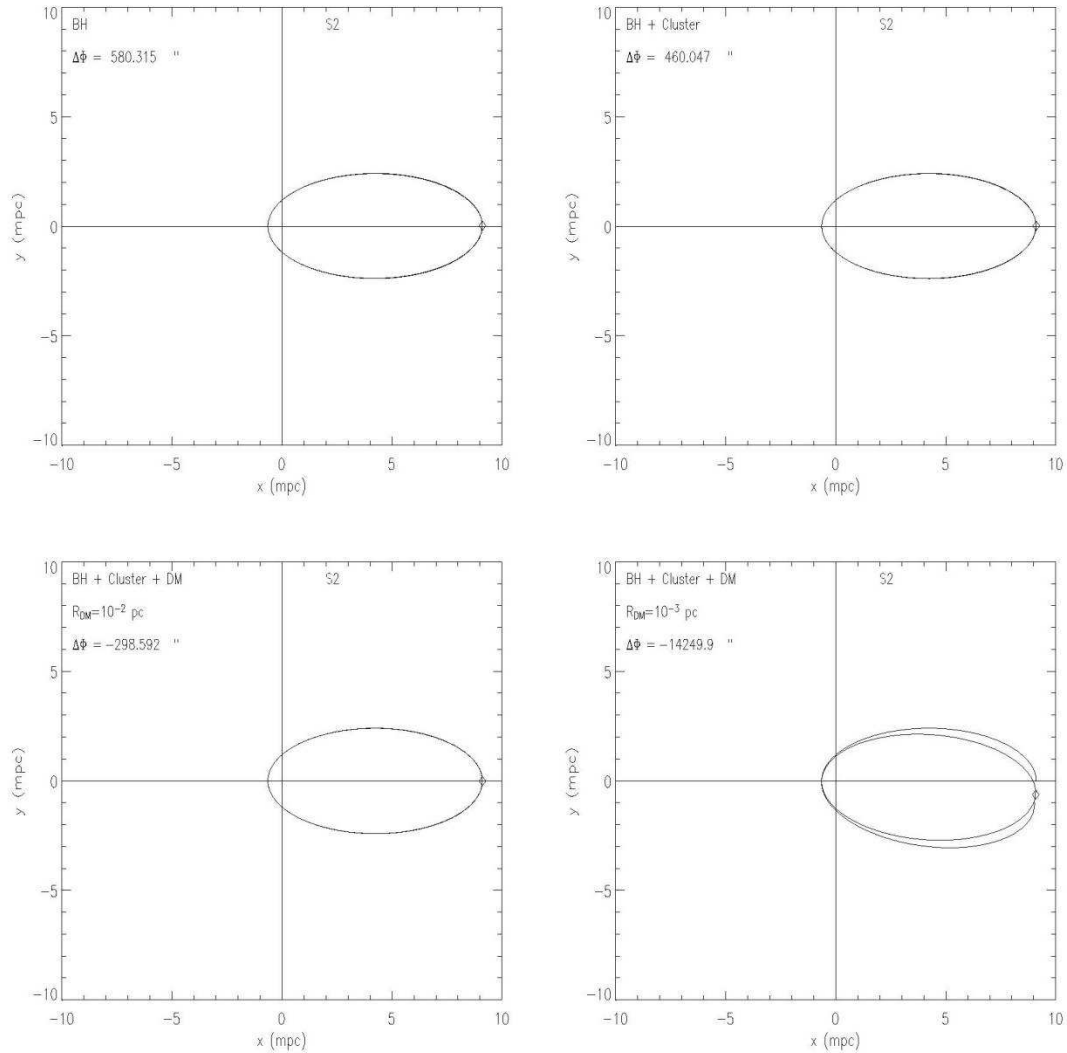
BH
S2
Δϕ = 580.315 "
BH + Cluster
S2
Δϕ = 460.047 "
BH + Cluster + DM
S2
R_DM=10^-2 pc
Δϕ = −298.592 "
BH + Cluster + DM
S2
R_DM=10^-3 pc
Δϕ = −14249.9 "
x (mpc)
y (mpc)

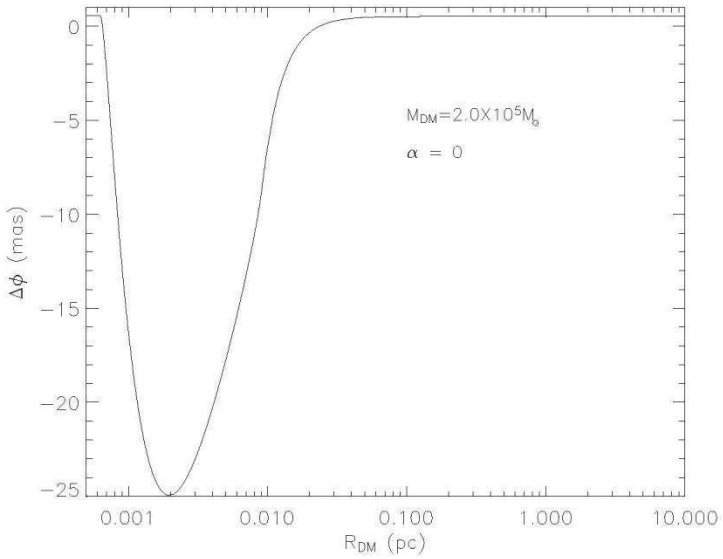

Figure 32: Apoastron shift as a function of the DM radius R_{DM} for $\alpha = 0$ and $M_{DM} \simeq 2 \times 10^5$ $M_\odot$. Taking into account present day precision for the apoastron shift measurements (about 10 mas) one can say that DM radii R_{DM} in the range $8 \times 10^{-4} - 10^{-2}$ pc are not acceptable.

D. Borka, P. Jovanovic, V. Borka Jovanovic and AFZ, PRD, **85**, 124004 (2012).

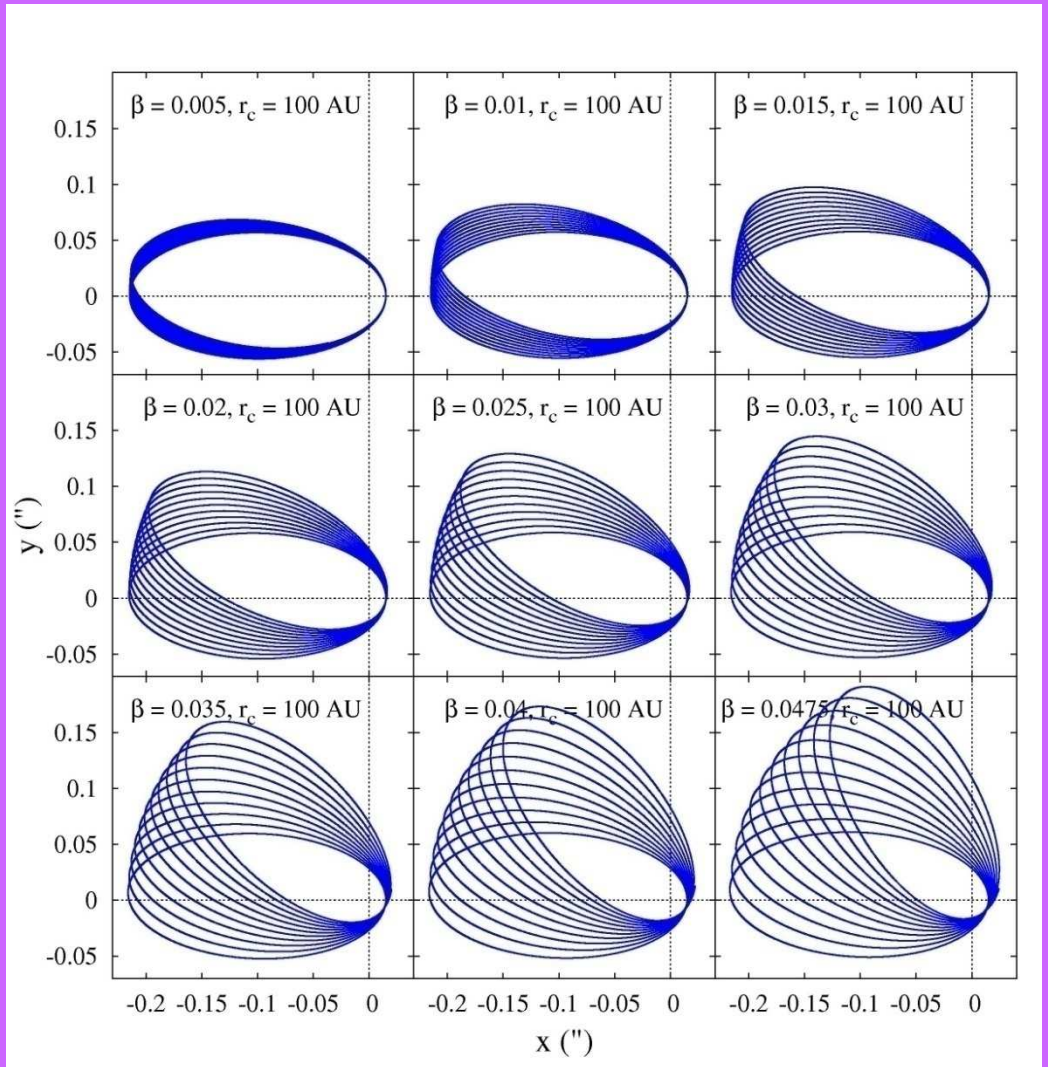

D. Borka, V. Borka Jovanovic, P. Jovanovic, AFZ

From an analysis of S2 orbit one can find signatures of Yukawa gravity (submitted)

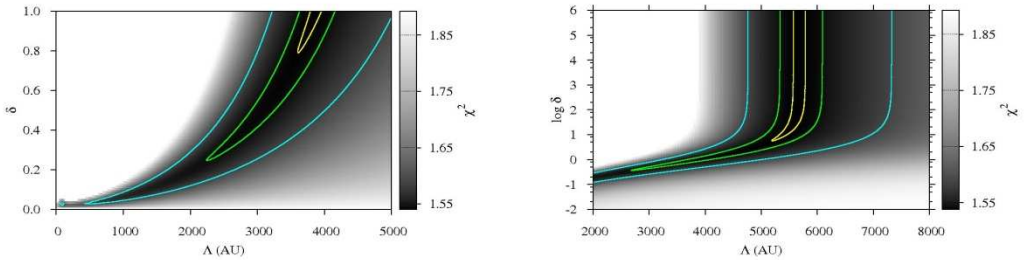

FIG. 7: **The maps of reduced χ^2 over the $\Lambda - \delta$ parameter space in case of NTT/VLT observations. The left panel corresponds to $\delta \in [0, 1]$, and the right panel to the extended range of $\delta \in [0.01, 10^6]$.** The shades of gray color represent the values of the reduced χ^2 which are less than the corresponding value in the case of Keplerian orbit, and three contours (from inner to outer) enclose the confidence regions in which the difference between the current and minimum reduced χ^2 is less than 0.0005, 0.005 and 0.05, respectively.

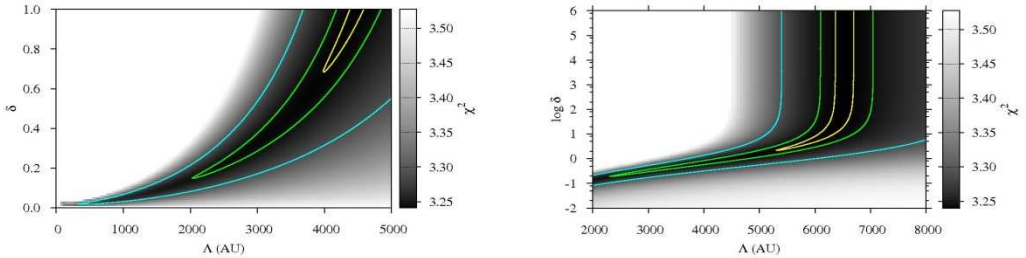

FIG. 8: **The same as in Fig. 7, but for the combined NTT/VLT+Keck observations.**

Yukawa gravity Λ which was varied from 10 to 10 000 AU. In the case of NTT/VLT observations the minimum of reduced χ^2 is 1.54 and is obtained for $\Lambda = 2.59 \times 10^3$ AU, while in the case of NTT/VLT+Keck combined data set the minimal value of 3.24 is obtained for $\Lambda = 3.03 \times 10^3$ AU. For both cases the reduced χ^2 for Keplerian orbits ($\delta = 0$) are 1.89 and 3.53, respectively, and thus significantly higher than the corresponding minima for $\delta = 1/3$. This means that Yukawa gravity describes observed data even better than Newtonian gravity and that $\delta = 1/3$ is valid value at galactic scales.

Figs. 7 and 8 present the maps of the reduced χ^2 over the $\Lambda - \delta$ parameter space for all simulated orbits of S2 star which give at least the same or better fits than the Keplerian orbits. These maps are obtained by the same fitting procedure as before. **The left panels of both figures correspond to $\delta \in [0, 1]$ and Λ[AU] $\in [10, 5000]$, and the right panels to the extended range of $\delta \in [0.01, 10^5]$ and Λ[AU] $\in [2000, 8000]$.** Three contours (from inner to outer) enclose the confidence regions in which the difference between the current and minimum reduced χ^2 is less than 0.0005, 0.005 and 0.05, respectively. **As it can be seen from Fig. 7, the most probable value for the scale parameter Λ, in the case of NTT/VLT observations of S2 star, is around 5000 - 6000 AU, while in the case of NTT/VLT+Keck combined data set (Fig. 8), the most probable value for Λ is around 6000 - 7000 AU. In both cases χ^2 asymptotically decreases as a function of δ, and hence, it is not possible to obtain reliable constrains on the universal constant δ of Yukawa gravity. Also, these two parameters δ and Λ are highly correlated in the range $(0 < \delta = +1/3 < 1)$. For $\delta > 2$ (the vertical strips) they are not correlated.**

As it could be also seen from left panels of Figs. 7 and 8, the values $\delta \approx 1/3$ result with very good fits for which the reduced χ^2 deviate from the minimal value for less than 0.005 (middle contours in both figures). The corresponding values for Λ range approximately from 2500 to 3000 AU. For $\delta = 1/3$ we obtained the following values: $\Lambda = 2590 \pm 5$ AU (NTT/VLT data) and $\Lambda = 3030 \pm 5$ AU (NTT/VLT+Keck combined data).

Although both observational sets indicate that the orbit of S2 star might be not a Keplerian one, the current astrometric limit is not sufficient to unambiguously confirm such a claim. However, the accuracy is constantly improving from around 10 mas during the first part of

- **Conclusions**

- VLBI systems in mm and sub-mm bands could detect mirages (“faces”) around black holes.
- Shapes of images give an important information about BH parameters
- Trajectories of bright stars or bright spots around massive BHs are very important tool for an evaluation of BH parameters
- Trajectories of bright stars or bright spots around massive BHs can be used to obtain constraints on alternative theories of gravity (f(R) theory, for instance)
- A significant tidal charge of the BH at GC is excluded by observations , but there signatures of extreme RN charge (perhaps non-electric one)

- Thanks for your kind attention!